

# Vulnerabilities in Partial TEE-Shielded LLM Inference with Precomputed Noise

Abhishek Saini

Rutgers, The State University of New Jersey  
Piscataway, NJ, USA  
abhishek.saini@rutgers.edu

Haolin Jiang

Rutgers, The State University of New Jersey  
Piscataway, NJ, USA  
hj462@scarletmail.rutgers.edu

Hang Liu

Rutgers, The State University of New Jersey  
Piscataway, NJ, USA  
hang.liu@rutgers.edu

## Abstract

The deployment of large language models (LLMs) on third-party devices requires new ways to protect model intellectual property. While Trusted Execution Environments (TEEs) offer a promising solution, their performance limits can lead to a critical compromise: using a precomputed, static secret basis to accelerate cryptographic operations. We demonstrate that this mainstream design pattern introduces a classic cryptographic flaw, the reuse of secret keying material, into the system’s protocol. We prove its vulnerability with two distinct attacks: First, our attack on a model confidentiality system achieves a full confidentiality break by recovering its secret permutations and model weights. Second, our integrity attack completely bypasses the integrity checks of systems like Soter and TSQP. We demonstrate the practicality of our attacks against state-of-the-art LLMs, recovering a layer’s secrets from a LLaMA-3 8B model in about 6 minutes and showing the attack scales to compromise 405B-parameter LLMs across a variety of configurations.

**CCS Concepts:** • Security and privacy → Key management; Cryptanalysis and other attacks; Domain-specific security and privacy architectures; • Computing methodologies → Natural language processing.

**Keywords:** Confidential Computing, Machine Learning Security, Trusted Execution Environments (TEEs), Large Language Models (LLMs), Cryptographic Attacks, Key Reuse

## 1 Introduction

The initial wave of Large Language Models (LLMs) has been dominated by centralized, API-based services [3, 24, 57]. However, this paradigm is rapidly giving way to a new frontier: local deployment of models outside the provider’s direct control. This shift is not driven by a single factor, but by three distinct and essential requirements: First, enterprise users are increasingly running models on-premises to process sensitive, proprietary data, driven by concerns over exposing market secrets to competitors and the legal and compliance risks of sharing confidential information with third-party model providers [58, 67]. Second, entire classes of mission-critical applications, such as autonomous driving and robotics, are non-negotiable edge-native; their need for real-time responsiveness and constant availability precludes any reliance on

a remote server [16, 19, 39, 77]. Finally, the proliferation of consumer devices like smartphones and smart assistants, now equipped with powerful AI accelerators, has created a demand for a new generation of responsive, always-on applications powered by local proprietary models [4, 26, 86].

While each requirement is distinct, they converge on a single, critical security challenge: placing a multi-million dollar model, a core intellectual property asset, onto hardware not managed by the provider exposes it to unauthorized replication and reverse engineering [76]. This tension has led to a clear call from the research community for a “middle path” that delivers the full benefits of local execution without sacrificing the model provider’s intellectual property [14, 33].

One approach to securing inference relies on purely cryptographic methods like Homomorphic Encryption (HE), which allow computation on encrypted data. However, HE is often too slow for the demands of low-latency LLM inference [22, 37]. Consequently, hardware-based solutions using Trusted Execution Environments (TEEs) have emerged as a more practical alternative that offers a better balance of security and performance [27, 55]. However, the memory and performance constraints of TEEs make running an entire state-of-the-art LLM within a secure enclave impractical [40, 45]. While recent confidential computing architectures like Intel TDX, AMD SEV, Arm CCA, and NVIDIA’s Confidential Computing are beginning to address these limitations, their practical adoption is hindered by limited availability or the persistent challenge of securing untrusted accelerators [1, 15, 17, 34, 38, 69, 82, 83, 96]. This has led to the mainstream paradigm of *Partial TEE-Shielded Execution (PTSE)*, which offloads computationally intensive operations to powerful but untrusted hardware like Graphics Processing Units (GPUs), while the TEE retains a critical role in managing the overall secure execution of the model [48, 68, 72, 75, 78].

Early PTSE strategies focused on model partitioning, where the model is split, and only the most sensitive layers or components are executed inside the TEE [49, 51, 65]. However, this strategy is flawed as it offers incomplete IP protection and underutilizes the accelerator [46, 74].

More recent PTSE approaches have evolved towards cryptographic obfuscation, which operates on a “lock-and-key” principle: The model is first obfuscated (locked) offline using a secret transformation, rendering it unusable by any

System	Security Goal	Masking Strategy (in TEE)	Offloaded Computation (on GPU)	Restoration Mechanism (in TEE)
ShadowNet [75]	Model Confidentiality	Additive one-time pad, $M$ , on the input feature map, $X$ : $X' = X + M$ .	Convolution with the transformed weights, $\hat{W}^T$ , and the masked input, $X'$ : $Y' = \text{Conv}(X', \hat{W}^T)$ .	Restores $Y$ by subtracting the pre-computed noise effect and applying an inverse weight transformation: $Y = (Y' - \text{Conv}(M, W)) \cdot \Lambda^{-1}$ .
SLIP [62]	Model Confidentiality	Additive one-time pad, $r_{i-1}$ , on the input activation, $a_{i-1}$ : $\tilde{a}_{i-1} = a_{i-1} + r_{i-1}$ .	Matrix-vector multiplication with matrix $W_i^D$ and the masked activation, $\tilde{a}_{i-1}$ : $\tilde{a}_i^D = W_i^D \cdot \tilde{a}_{i-1}$ .	Restores $a_i^D$ by subtracting precomputed cancellation mask, $c_i$ : $a_i^D = \tilde{a}_i^D - c_i = W_i^D a_{i-1}$ , where $c_i = W_i^D r_{i-1}$ .
Soter [68]	Model Confidentiality	Parameter Morphing: Multiplies the linear operator $F$ with a secret scalar blinding coin, $\mu$ .	The morphed operator is executed on the GPU with plaintext input: $\mu \cdot F(X)$ .	Restores $F(X)$ by multiplying the result by the reciprocal of the blinding coin: $\mu^{-1} \cdot (\mu \cdot F(X)) = F(X)$ .
TransLinkGuard (TLG) [48]	Model Confidentiality	Additive one-time pad, $m$ , on the input activation $a'$ , followed by a permutation $\rho_l$ : $a'' = (a' + m)\rho_l$ .	Matrix-vector multiplication with matrix, $W_3'$ , and masked, permuted input, $a''$ : $b'' = a'' W_3'$ .	Restores $b$ by subtracting the precomputed noise effect, $mW_b$ : $(b'' - mW_b) = b$ .
Soter [68], TSQP [74]	Computational Integrity	Challenge Injection: Injects a fingerprint vector $m'$ , a random linear combination of a static basis of cornerstone inputs, $\{m_i\}$ : $m' = \sum \alpha_i m_i$ .	The GPU computes the linear operation $F$ on a batch containing both genuine activations and the fingerprint challenge, producing $F(m')$ .	Result Verification: TEE computes the expected output, $F(m')$ , using linearity of $F$ and precomputed cornerstone outputs, $\{F(m_i)\}$ , $F(m') = \sum \alpha_i F(m_i)$ and compares it to GPU's result.

**Table 1.** The mask-offload-restore pattern in practice across TEE-shielded inference systems.

party that does not possess the corresponding secret key. During online inference, the TEE’s role is twofold: (i) Model confidentiality. TEE guards the model’s secrets by securely holding the key needed to de-obfuscate computations from the GPU. A common approach to obfuscation in this domain is permutation-based locking, which secretly shuffles a model’s weights; the TEE then ensures the model only functions correctly by using the secret permutation key to properly order the data flowing into the locked model weights [48, 75, 84, 87, 91, 94]. Recent work has focused on scaling this approach to protect LLMs [48, 62, 74, 84]. (ii) Computational integrity. The TEE serves to verify the integrity of computations offloaded to an untrusted hardware. This is a vital role, as an attacker with control over the host system could manipulate the GPU’s computations. Such tampering can degrade the model’s service quality, damaging the provider’s reputation and eroding user trust. More maliciously, even an unprivileged, co-located attacker could aim for targeted manipulations [29, 41], altering the computation in subtle ways to bypass security filters or cause specific misclassifications that benefit them [61, 95]. To prevent this, systems like Soter [68] and TSQP [74] leverage the TEE hardware to inject hidden *fingertprints*, known-answer challenges for which the TEE already knows the correct output, mixed in with real data. If the untrusted hardware returns a tampered result for these hidden checks, the integrity breach is detected, and the session can be determined as untrusted.

To achieve these distinct security goals, a common architectural pattern has emerged across a wide range of systems: a three-step *Mask-Offload-Restore* protocol, which we detail and compare across several state-of-the-art systems in Table 1. The protocol proceeds as follows:

1. **Mask.** Inside the TEE, plaintext data is cryptographically masked. For confidentiality, this involves adding secret noise to an input; for integrity, it involves injecting a known-answer fingerprint challenge.

2. **Offload.** The masked data is then offloaded to an untrusted hardware (e.g., GPU), which performs the computationally expensive linear operations.
3. **Restore.** The result is returned to the TEE, which must efficiently restore the plaintext output by removing the noise’s effect or verify the computation’s integrity by checking the fingerprint’s result.

The practical challenge arises because the TEE is responsible for more than just generating this randomness; it must also restore the original result by computing the precise effect of the noise. As we will demonstrate in Section 3, calculating this effect for truly random noise is computationally prohibitive. It would force the TEE to execute expensive *On-the-Fly* operations, like full matrix-vector multiplications, creating an unacceptable performance bottleneck.

To circumvent this bottleneck, practical implementations are compelled to adopt a performance-driven shortcut: a *precomputation*-based pattern. At startup, the TEE generates and stores a small, fixed set of  $K$  secret noise vectors and their corresponding effects, which we call the precomputed static basis. During online inference, all “random” noise is then efficiently generated by combining these precomputed static basis vectors using freshly sampled random coefficients. For TEE-based model confidentiality, this efficiency-driven design is a necessity to scale to LLMs, while for others, like the integrity-checking mechanism in Soter, TSQP, it is adopted as a tempting shortcut for efficiency.

In this work, we demonstrate that this efficiency-driven reliance on a precomputed static basis is a fundamental security flaw. The key insight is that the random noise generated this way is not truly random. Instead, it is permanently confined to a predictable, low-dimensional ( $K$ -dimensional) subspace spanned by the static basis vectors. This creates a critical vulnerability that allows an attacker to aggregate information over multiple interactions to algebraically break the system’s

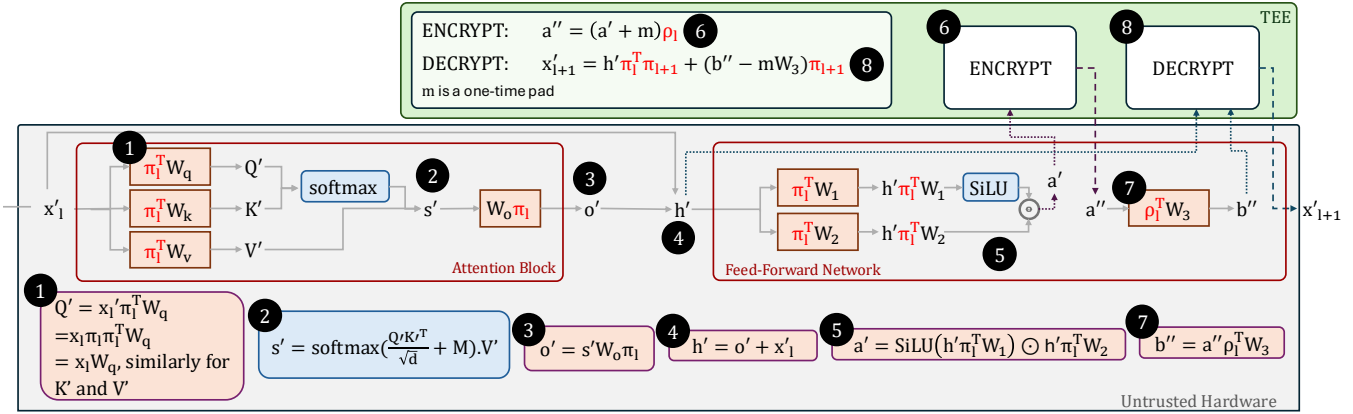


Figure 1. Activation flow in a Llama transformer layer secured using TLG [48].

security guarantees. This flaw is not an implementation bug or a side channel, but a systematic weakness inherent to the protocol’s design.

We prove the severity of this flaw by developing attacks that compromise two distinct security guarantees: model confidentiality system and computational integrity framework. The success of our attacks on these two different real-world designs proves that the static basis is a versatile and fundamental vulnerability. Our primary contributions are:

- The identification of the “static secret basis” pattern as a critical, performance-driven vulnerability in TEE-shielded inference systems.
- The development and formalization of a novel attack that breaks model confidentiality in systems like TLG [48] by algebraically characterizing the noise subspace to recover secret permutations.
- The development of a more general attack that bypasses integrity protection in systems like Soter [68], TSQP [74] by isolating the hidden noise subspace from other data through vector space intersection.
- An extensive evaluation that validates the effectiveness of our attacks. We demonstrate that the underlying vulnerability stems from a necessary performance trade-off. Our methods are robust and scalable to state-of-the-art LLM models across various configurations.

**Distinction from existing closely related attacks.** While other protocol-level Partial TEE-shielded execution attacks exist, they typically rely on statistical inference and require a known public model to succeed [84, 93, 94]. Our attack is fundamentally different from prior work. We exploit a mathematical flaw in the security protocol itself, assuming a perfect TEE. Our attack can perfectly isolate the reused secret basis, enabling attackers to fully obtain the protected LLM model and bypass integrity checks, demonstrating a new manifestation of key-reuse vulnerability in partial TEE-shielded executions. Please refer to Section 7 for more discussions.

## 2 Background and Threat Model

### 2.1 TEE-based Model Confidentiality

Many TEE-based model confidentiality schemes operate on a lock-and-key authorization principle to enable secure computation on untrusted hardware [5, 46, 48, 68, 75, 84, 87]. In this paradigm, the model’s weights are first “locked” offline through an obfuscation technique, such as permutation, rendering them unusable without a corresponding secret key. This locked model is then deployed to the untrusted environment. The secret key, the permutation matrix in this case, is stored securely within the TEE. During inference, TEE uses the secret key to securely perform the secret transformation necessary for the correct functioning of the model.

As a concrete example of this mechanism, Figure 1 illustrates a single layer of the Llama architecture secured using TLG [48]. In the secured model, the weights are locked offline using layer-specific permutation matrices,  $\pi_l$  and  $\rho_l$ . To an attacker, these locked weights appear random; they are unusable without the secret permutations, which are stored securely in the TEE. We denote secured activations with a prime (e.g.,  $x'_l$ ) to distinguish them from their plaintext counterparts ( $x_l$ ).

The inference process works by applying corresponding permutations to the activations. An incoming activation  $x'_l$ , already permuted by the previous layer ( $x'_l = x_l \pi_l$ ), is processed by the attention block. Due to the block’s structure, the permutations on the weights and activations cancel out at step 1, ensuring the intermediate outputs are correct (e.g.,  $Q' = x'_l \pi_l^T W_q = (x_l \pi_l) \pi_l^T W_q = Q$ ).

The computed values  $Q'$ ,  $K'$ ,  $V'$  are then combined to form the aggregated context,  $s'$  (2), which then gets multiplied by the output projection matrix,  $W_o \pi_l$  (3). This gives the output of the attention block,  $o'$ . A residual connection is added to create  $h'$  (4), the input to the feed-forward network. At this stage,  $h' = h \pi_l$  is permuted correctly for the first half of the feedforward network to compute  $a'$  (5). Since  $h'$  cancels out the permuted weights of the first half of the

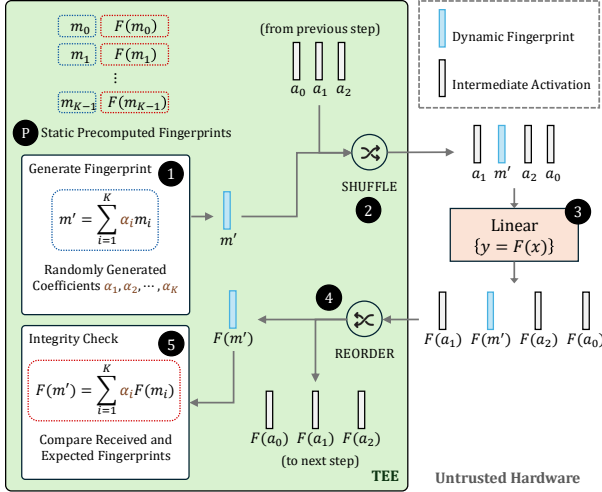


**Figure 2.** Soter’s mechanism for generating integrity fingerprints from a static basis of precomputed cornerstones.

feed-forward network,  $a'$  is the same as its plaintext version  $a$ . Therefore,  $a'$  is not correctly permuted for the locked weight  $W'_3 = \rho_l^T W_3$ . To securely apply the required permutation  $\rho_l$  without leaking it to an observer, the system uses a three-step ENCRYPT-LINEAR-DECRYPT sequence: the TEE first encrypts the activation  $a'$  with a random one-time pad ( $m$ ) before permuting it (6), the GPU performs the linear computation (7), and TEE decrypts the result by removing the noise effect ( $mW_3$ ) to recover the correct output (8).

To ensure the cryptographic security of one-time pad masking, all computations are performed over a finite field. Following standard practice, all floating-point activations and weights are first quantized to fixed-point integers. These integers are then treated as elements of the finite field  $\mathbb{F}_P$ , where  $P$  is a large prime chosen to prevent wrap-around errors. This step is what allows the random mask  $m$  to function as a secure one-time pad, providing a formal basis for the system’s security guarantees [78].

## 2.2 TEE-based Computational Integrity

Model’s computational integrity is sometimes protected using a technique called *oblivious fingerprinting* [68, 74]. The core idea is to mix known-answer fingerprints, challenges for which the TEE already knows the correct output, with the genuine user inputs sent to the GPU. To prevent an attacker from simply detecting and ignoring these checks, the fingerprints are designed to be statistically indistinguishable from normal inputs. By verifying the GPU’s output for these hidden fingerprints, the TEE can detect any tampering.

Figure 2 exemplifies this mechanism used in Soter [68] and TSQP [74]. Beginning with a one-time offline setup where the TEE creates and stores a static basis of  $K = 10$  cornerstone fingerprint pairs,  $\{m_i, F(m_i)\}$  (P). During each online inference, the TEE generates a dynamic challenge,

$m'$ , as a random linear combination of the cornerstone inputs ( $m' = \sum_{i=1}^K \alpha_i m_i$ ) (1). This challenge is then shuffled with genuine activations and sent to the GPU (2), which applies the operator  $F$  to the entire batch (3). Upon receiving the results, the TEE unshuffles them (4) and verifies the GPU’s work by comparing the returned fingerprint output,  $F(m')$ , against the expected result it computes locally:  $F(m')_{expected} = \sum_{i=1}^K \alpha_i F(m_i)$  (5). A mismatch signifies an integrity breach and aborts the process.

## 2.3 Threat Model

We consider a setting where a defender (model provider) deploys a proprietary model on a user’s device, which is controlled by a powerful adversary. The defender’s goal is to guarantee two security properties for the deployed model: model confidentiality, to protect the intellectual property of its weights and parameters, and computational integrity, to verify the correctness of any computation offloaded to untrusted hardware.

We assume the TEE itself is a secure black box, free from physical or hardware side-channel attacks. All components outside the TEE including the host operating system, system memory, and the GPU accelerator are considered untrusted and are fully controlled by the adversary. The adversary’s capabilities are therefore formidable: they can observe, intercept, and modify all communication between the TEE and the untrusted GPU. They know the complete architecture of the deployed model and the full details of the security protocol being used, but they do not have access to the secret keying material (e.g., secret permutations, static noise basis) held within the TEE. The adversary’s objective is to break the defender’s security guarantees. Aligned with our two primary case studies, we define two concrete goals for the adversary: (1) to compromise confidentiality by recovering the secret keys needed to fully reconstruct the original model (as in a TLG-like system), or (2) to compromise integrity by identifying and bypassing the verification mechanism to tamper with results without detection (as in Soter).

## 3 Key Observations on the Trade-off between Security vs Computation Cost

### 3.1 Key Observations

**Observation 1:** TLG authorization process critically hinges on the TEE’s ability to efficiently calculate the noise effect  $mW_3$ .

Analyzing the workflow of TLG, we observe that the computations inside the TEE (6 and 8 in Figure 1) can lead to a bottleneck. In particular, the calculation of the noise effect,  $mW_3$ , should be efficient since it has the largest computational footprint. In the meantime, as the model continues to grow (e.g., LLM), and the deployment of these LLMs on mobile devices becomes prevalent [48, 70], the memory cost mainly surrounding  $W_3$  could also be a concern (Table 3).

**Observation 2:** Soter's design relies on the use of a static basis of precomputed fingerprints to efficiently calculate the fingerprint's expected output  $F(m')$ .

This observation highlights a fundamental tension in Soter's design. For the integrity mechanism to be secure, the dynamically generated fingerprints must be statistically indistinguishable from genuine activations. However, for the mechanism to be efficient, Soter relies on this static, precomputed basis to enable rapid integrity checks, a point acknowledged in the original paper [68]. As we show later in the paper, this reliance on a static basis forces all generated fingerprints into a predictable, low-dimensional subspace, making them computationally distinguishable from genuine inputs and undermining the system's security guarantee.

In summary, the mechanisms in our two case studies, TLG and Soter, share a critical dependency: the need for an efficient TEE-based calculation of a noise effect ( $mW_3, F(m')$ ). As we will detail in Section 3.2, there are two main strategies to compute this effect: an on-the-fly method that generates fresh randomness for each query, versus a more performant precomputation-based approach that relies on a static, pre-loaded table of noise vectors. However, the prohibitive memory and latency costs of the on-the-fly method force designers to adopt the precomputation-based approach, as shown in our subsequent detailed analysis of a TLG-like system.

### 3.2 Detailed Analysis

This section uses TLG to explain the on-the-fly vs precomputed approaches with the memory and latency constraints in consideration.

**On-the-Fly Approach** employs an ENCRYPT-LINEAR-DECRYPT sequence to authorize computations on the untrusted platform. As illustrated in Figure 3(a), the TEE first ENCRYPTs (6) an activation by masking it with a random One-Time Pad (OTP),  $m$ . After the LINEAR computation is performed on the GPU (7), the result re-enters the TEE. The DECRYPT function (8) then recovers the correct output by subtracting the effect of the initial noise,  $mW_3$ . The method used to obtain this noise effect,  $mW_3$ , (6.2) is the most time-consuming operation across the entire sequence.

The on-the-fly approach first randomly generates the noise vector  $m$  (6.1). To calculate the corresponding noise effect  $mW_3$ , the entire permuted weight matrix,  $\rho_l^T W_3$ , must be copied from untrusted memory into the TEE (2), where the matrix-vector multiplication is performed (6.2). However, this approach is inefficient as  $W_3$  imposes (i) high memory demand and (ii) significant processing latency in the TEE.

(i) *Memory demand* per layer—given by  $d_{in} \times d_{out} \times s_{dtype}$  (matrix dimensions times datatype size)—often exceeds the capacity of memory-constrained TEEs. In LLaMA-3-8B model, for example,  $W_3$  requires 112 MB in bfloat16, which doubles to 224 MB when converted to 32-bit integers required for

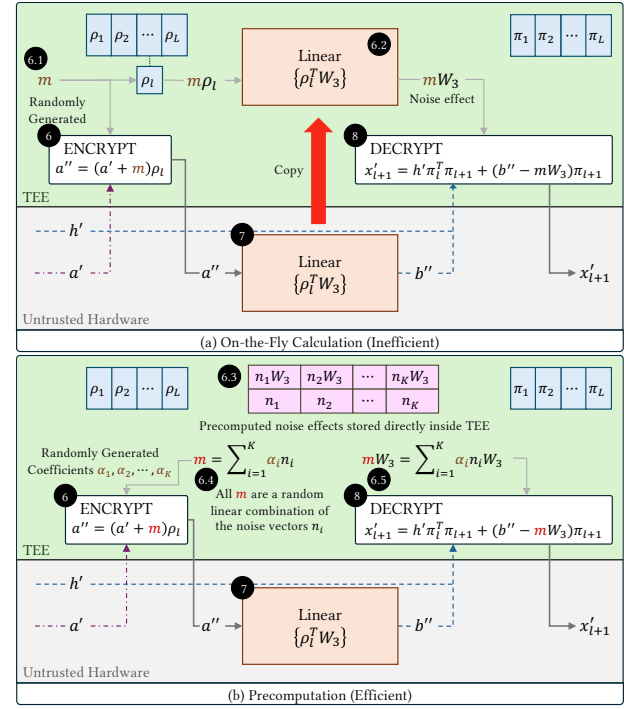


**Figure 3.** A comparison of two methods for calculating noise effects inside the TEE. (a) The on-the-fly approach. (b) The precomputation approach.

TEE Technology	Architectural Model	Available Memory	Bottleneck
SGX v1	Application Isolation	Small, static EPC (e.g., 128 MB)	Memory and compute.
SGX v2	Application Isolation	Small (e.g., 128 MB) on clients; Large (GBs) on servers.	Memory and compute on clients; Compute on servers.
ARM TrustZone	System Partitioning	Small, fixed DRAM (16-64 MB)	Memory and compute.
AMD SEV-SNP	Hardware-Isolated VM	Large, dynamic protected memory (GBs)	Primarily compute.
Intel TDX	Hardware-Isolated VM	Large, dynamic protected memory (GBs)	Primarily compute.
ARM CCA	Hardware-Isolated VM	Large, dynamic protected memory (GBs)	Primarily compute.

**Table 2.** Memory constraints comparison across representative TEE technologies.

Model Family	Model Size	FFN Dim ( $d_{in}$ )	Hidden Dim ( $d_{out}$ )	$W_3$ Memory
LLaMA-3	8B	14,336	4,096	$\approx$ 224 MB
Gemma 3	27B	21,504	5,376	$\approx$ 441 MB
LLaMA-3	70B	28,672	8,192	$\approx$ 896 MB
Mistral Large 2	123B	28,672	12,288	$\approx$ 1.31 GB
LLaMA-3.1	405B	53,248	16,384	$\approx$ 3.25 GB

**Table 3.** Architectural parameters and memory footprint of the  $W_3$  matrix in recent open-source LLM families.

6.2, getting close to the memory limits of typical SGX and ARM TrustZone platforms (see Table 2). Moreover, this footprint grows substantially for larger models (Table 3), making memory a critical bottleneck for on-the-fly approaches. We

also want to mention that in modern server-based TEEs (e.g., Intel SGX v2, Intel TDX, AMD SEV-SNP, ARM CCA), one can have 10s of GB of memory that can hold large LLMs.

(ii) *Significant latency* is the key concern that derails the on-the-fly approach. Particularly, the latency  $T_{\text{fly}}$  contains two parts: (i) memory copy latency ( $\frac{d_{\text{in}} \times d_{\text{out}} \times s_{\text{dtype}}}{BW_{\text{tee}}}$ ) and (ii) CPU computation latency ( $\frac{2 \times d_{\text{in}} \times d_{\text{out}}}{\text{FLOPS}_{\text{cpu}}}$ ), where  $BW_{\text{tee}}$  is the TEE memory bandwidth and  $\text{FLOPS}_{\text{cpu}}$  the in-enclave CPU performance. Therefore,  $T_{\text{fly}} = \left( \frac{s_{\text{dtype}}}{BW_{\text{tee}}} + \frac{2}{\text{FLOPS}_{\text{cpu}}} \right) \times d_{\text{in}} \times d_{\text{out}}$ . Our benchmarks show that for the LLaMA-3-8B model, CPU computation alone exceeds 70 ms per layer, resulting in more than 2 s per token in a 32-layer model, which is too slow for low-latency applications. As  $W_3$  increases in larger architectures (Table 3), the latency scales proportionally and becomes even more severe. For the LLaMA-3.1-405B model, the CPU computational latency approaches 1 second per layer. This will render a per-token latency up to 32 seconds.

**Precomputation-based Approach**, shown in Figure 3(b), addresses these bottlenecks by replacing costly matrix multiplications with lightweight linear combinations. Instead of loading  $W_3$  into the TEE, a small table of  $K$  basis noise vectors  $\{n_1, \dots, n_K\}$  and their precomputed effects  $\{n_1 W_3, \dots, n_K W_3\}$  (6.4) is prepared at startup. During inference, the TEE samples random coefficients  $\{\alpha_1, \dots, \alpha_K\}$  to construct both the noise vector  $m = \sum_{i=1}^K \alpha_i n_i$  (6.4) and its effect  $mW_3 = \sum_{i=1}^K \alpha_i \times (n_i W_3)$  (6.5), thereby avoiding on-the-fly multiplications.

This design reduces both memory and latency to practical levels. The memory footprint is now determined by the size of this precomputed table, which must store the  $K$  basis noise vectors (each of dimension  $d_{\text{in}}$ ) and their  $K$  resulting effects (each of dimension  $d_{\text{out}}$ ). The memory cost becomes  $K \times (d_{\text{in}} + d_{\text{out}}) \times s_{\text{dtype}}$ , which is orders of magnitude smaller since  $K \ll d_{\text{out}}$ . Similarly, the latency is also significantly lower than in the on-the-fly approach. For the LLaMA-3-8B model with  $K = 10$ , the per-layer footprint drops from  $\sim 224$  MB to  $\sim 0.7$  MB ( $> 300 \times$  reduction), while latency decreases from 70 ms to 0.23 ms per layer ( $\sim 300 \times$  reduction).

**The choice of  $K$ .** Intuitively, increasing  $K$  enhances security by introducing more randomness. In practice, however,  $K$  is limited by both memory and latency constraints: First, the precomputed table across all  $L$  layers must fit within the TEE’s memory budget  $M_{\text{tee}}$ , giving:

$$L \times K_0 \times (d_{\text{in}} + d_{\text{out}}) \times s_{\text{dtype}} \leq M_{\text{tee}}, K_0 \leq \frac{M_{\text{tee}}}{L \times (d_{\text{in}} + d_{\text{out}}) \times s_{\text{dtype}}}.$$

Second, the in-enclave computation across all  $L$  layers must not exceed the overall latency budget ( $T_{\text{budget}}$ ), giving:

$$L \times \frac{2 \times K_1 \times (d_{\text{in}} + d_{\text{out}})}{\text{FLOPS}_{\text{cpu}}} \leq T_{\text{budget}}, K_1 \leq \frac{T_{\text{budget}} \times \text{FLOPS}_{\text{cpu}}}{2 \times (d_{\text{in}} + d_{\text{out}})}.$$

In a practical deployment,  $K$  must satisfy both constraints, making the true maximum basis size  $K_{\text{max}} = \min(K_0, K_1)$ .

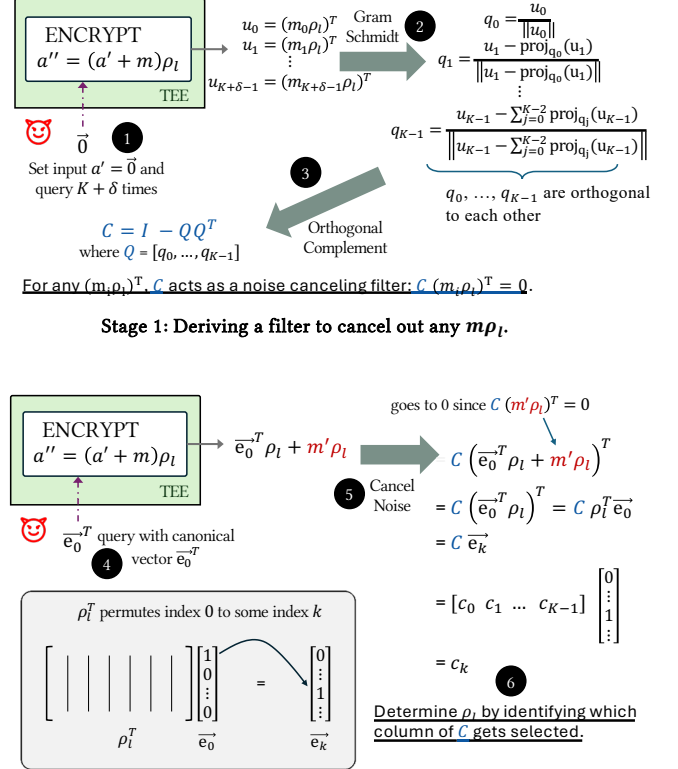


**Figure 4.** An illustration of the two-stage attack to reveal  $\rho_l$  of (6) in Figure 3(b).

For LLaMA-3 8B on a 128 MB TEE, the memory constraint alone bounds  $K_{\text{max}} \approx 56$  in a TLG-like system, with the actual value  $K$  necessarily set even lower to reserve space for runtime data and secrets.

The memory and latency constraints force  $K$  to be small, which creates a low-rank vulnerability that our attacks exploit. These constraints are inherent to TEEs and therefore apply to all precomputation-based approaches. For example, Soter uses a static basis of  $K = 10$  fingerprints to achieve integrity checking with low latency and acceptable memory overhead. To demonstrate the severity and generality of this flaw, we next present two attacks: first on a TEE-based model confidentiality protocol (Section 4), and second on a TEE-based integrity checking mechanism (Section 5).

## 4 Attack on TEE-based Model Confidentiality

This section presents an attack on the TEE-based model confidentiality protocol of a TLG-like system that uses a static precomputed basis of noise vectors due to the practical constraints discussed in Section 3. The attack ultimately results in the full leak of the model weights.

## 4.1 Attack Formalization

The attack compromises the model layer by layer. For a given layer  $l$ , a full break requires recovering its two secret permutation matrices:  $\rho_l$  (6 in Figure 3) and  $\pi_{l+1}$  (8 in Figure 3), which authorizes the output for the subsequent layer. Note that as part of this layer-wise procedure, permutation  $\pi_l$  is not a target when attacking layer  $l$ , as it would have already been compromised during the attack on the preceding layer,  $l - 1$ . Additionally, for the initial layer ( $l = 1$ ),  $\pi_1$  is recovered directly from the model's input stage. An attacker can observe the permuted token embeddings, which must be transformed by  $\pi_1$  to align correctly with the first layer's locked weights. With  $\pi_1$  known, the attack can proceed. The process for recovering each layer's secret matrices ( $\rho_l$  and  $\pi_{l+1}$ ) then consists of two main steps:

- **Stage 1: deriving a filter to cancel out  $m\rho_l$ .** The attacker first learns the basis of the  $K$ -dimensional permuted noise subspace that spans  $m\rho_l$ . This is achieved by querying the ENCRYPT function  $K + \delta$  times with a zero-vector input to gather enough samples of the noise (Stage 1 of Figure 4).
- **Stage 2: Reveal the secret permutation  $\rho_l$ .** With the noise-canceling filter from Stage 1,  $m\rho_l$  can be canceled out, leaving only  $a'\rho_l$ . The attacker queries the ENCRYPT function  $d$  more times, once for each canonical basis vector (e.g.,  $\vec{e}_1, \vec{e}_2, \dots, \vec{e}_d$ ) to reveal where each input dimension is permuted, thereby reconstructing the entire permutation matrix  $\rho_l$  (Stage 2 of Figure 4).

**Reveal  $W_3, \pi_{l+1}, W_q, W_k, W_v, W_o, W_1$  and  $W_2$ .** After  $\rho_l$  is revealed, we can reveal  $W_3$  in 7. Finally, one can set  $h' = 0$  to reveal  $\pi_{l+1}$  in 8 in Figure 3(b) using the same procedure as that used for revealing  $\rho_l$ . This reveals  $W_q, W_k, W_v, W_o, W_1$  and  $W_2$  for layer  $l + 1$ . For a model with  $L$  transformer layers, an attacker can repeat this step for all layers to recover all secret permutations and fully unlock the model.

**4.1.1 Stage 1: Extracting the Subspace Basis for  $m\rho_l$ .** The first stage of the attack is to characterize the  $K$ -dimensional subspace containing the permuted noise vectors  $m\rho_l$  and construct a noise-canceling filter. This is possible because the noise vector  $m$  is not truly random but is always a linear combination of  $K$  secret basis vectors,  $m = \sum_{i=1}^K \alpha_i n_i$ . Consequently, the output  $m\rho_l$  is always confined to a predictable, low-dimensional subspace. The attacker proceeds with the following steps (see Figure 4):

1. Query for noise samples: The attacker queries the ENCRYPT function  $K + \delta$  times using a zero-vector input,  $a' = \vec{0}^T$ . The function returns  $K + \delta$  permuted noise samples as  $1 \times d$  row vectors,  $m_i\rho_l$ . The attacker transposes these into a set of  $d \times 1$  column vectors, which we denote as  $\{u_i = (m_i\rho_l)^T\}_{i=0}^{K+\delta-1}$ .

2. 2 Derive orthonormal basis: Using the collected column vectors  $\{u_i\}$ , the attacker applies the Gram-Schmidt process to compute an orthonormal basis for the subspace spanned by permuted noise,  $m\rho_l$ . This results in a  $d \times K$  matrix  $Q = [q_0, q_1, \dots, q_{K-1}]$ , whose columns span the subspace.
3. 3 Construct noise-canceling filter: The attacker uses this basis to construct a  $d \times d$  projection matrix,  $C = I - QQ^T$ . This matrix projects any vector onto the orthogonal complement of the noise subspace, acting as a perfect noise-canceling filter. For any collected noise vector  $u_j = (m_j\rho_l)^T$ , it holds that  $Cu_j = 0$ .

**4.1.2 Stage 2: Extracting the Permutation Matrix  $\rho_l$ .** In the second stage, the attacker uses the noise-canceling filter  $C$  to reveal the secret permutation  $\rho_l$  one mapping at a time. The reveal of the first mapping using the first canonical vector  $\vec{e}_0 = [1, 0, 0, \dots]^T$  is illustrated in Figure 4:

4. Query with a canonical vector: The attacker queries the ENCRYPT function with the first canonical basis vector as input,  $a' = \vec{e}_0^T$ . The function returns the row vector  $(\vec{e}_0^T \rho_l + m'\rho_l)$ .
5. Apply the filter: The attacker transposes this output into a column vector,  $v = (\vec{e}_0^T \rho_l)^T + (m'\rho_l)^T$ , and applies the projection matrix:

$$\begin{aligned} Cv &= C((\vec{e}_0^T \rho_l)^T + (m'\rho_l)^T) \\ &= C(\vec{e}_0^T \rho_l)^T + C(m'\rho_l)^T. \end{aligned}$$

Since the noise term  $C(m'\rho_l)^T$  is nullified by the filter, the result is only the projected signal:

$$Cv = C(\vec{e}_0^T \rho_l)^T.$$

6. Reveal the mapping: The term  $(\vec{e}_0^T \rho_l)^T = \rho_l^T \vec{e}_0$  is itself a canonical column vector, which we can call  $\vec{e}_k$ . The final result is thus  $C\vec{e}_k$ , which is equivalent to the  $k$ -th column of the matrix  $C$ . By observing the resulting vector and matching it to the corresponding column of the matrix  $C$ , the attacker can determine the index  $k$ . This reveals one mapping of the secret permutation:  $\rho_l^T$  maps index 0 to index  $k$ .

By repeating this process for all other canonical vectors  $(\vec{e}_1, \dots, \vec{e}_{d-1})$ , the attacker can recover the entire secret permutation matrix  $\rho_l$ . This two-stage process of characterizing the noise subspace and then filtering it to isolate the signal is formalized in Appendix D - Algorithm 1.

## 4.2 Discussion on sampling strategy, $K$ and $\delta$

Even if the TEE uses a complex strategy to combine the noise vectors, such as combining a random subset of the basis vectors for each query, the output  $m\rho_l$  is still confined to the same  $K$ -dimensional subspace, making the system vulnerable. We experimentally demonstrate this in Section 6.5.

$K$  is a protocol parameter chosen by the model provider during the offline noise table precomputation step. Our threat model assumes the attacker has full knowledge of the protection protocol, including  $K$ , except for the secret keys and permutations. However, even if the attacker does not know  $K$ , it can be found empirically by collecting outputs and observing the rank of the resulting vector set until it stabilizes. We confirm the practicality of the attack under unknown  $K$  (Section 6.3), demonstrating that the attack succeeds even when  $K$  is initially unknown. Discovery of  $K$  is possible because the rank is guaranteed to stabilize at  $K$  since  $m\rho$  is generated from a fixed  $K$ -dimensional subspace.

Our protocol assumes that a linear combination of all  $K$  vectors is used to generate the noise mask. Therefore, by querying  $K + \delta$  times, the attacker observes enough samples of the permuted noise subspace to derive its basis,  $Q$  (2) in Figure 4). The small constant  $\delta > 0$  is chosen to avoid the pathological case when some of the random combinations are linearly dependent by pure chance.

For a  $K \times K$  matrix whose entries are chosen uniformly at random from a finite field with  $P$  elements, the probability of it being rank deficient (linearly dependent) is:

$$P(\text{rank deficient}) = 1 - \prod_{i=1}^K \left(1 - \frac{1}{P^i}\right).$$

A derivation for this result has been provided in Appendix A. In our implementation of LLaMA-3-8B model, we used  $P = 2^{31} - 1$  for which this probability is negligible. So  $\delta$  can be something small like 1 or 2.

## 5 Attack on TEE-based Computational Integrity

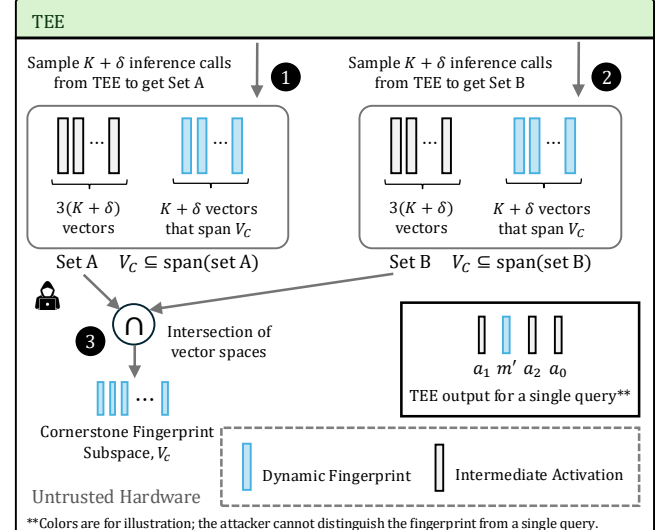
In this section, we show an attack that fully compromises a TEE-based integrity checking mechanism. In particular, we use Soter [68] as an example to explain the attack, although the same mechanism is also used in TSQP [74].

### 5.1 Attack Formalization

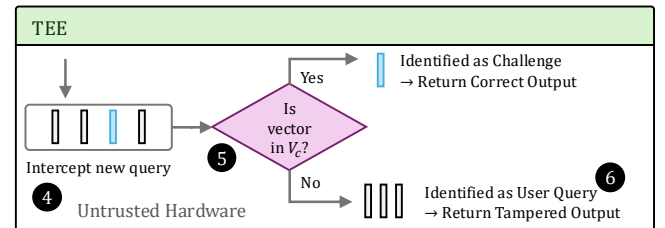
Soter protects computational integrity by mixing hidden, known-answer challenge fingerprints among genuine activations. By verifying the GPU’s computation on these challenges, the TEE can detect any tampering. The attacker’s goal, therefore, is to distinguish these challenge fingerprints from the genuine data. Doing so would allow the attacker to pass the integrity check by computing the challenges correctly while selectively tampering with genuine activations. The attack works in two stages as illustrated in Figure 5:

**Stage 1: Revealing the subspace for  $m_i$ .** In the first stage, the adversary learns a basis for the  $K$ -dimensional cornerstone fingerprint subspace, which we denote as  $V_C$ .

**Stage 2: Identifying the fingerprint to bypass the integrity check.** Armed with a basis for  $V_C$ , the adversary can



**Stage 1: Cornerstone fingerprint subspace recovery via intersection.**



**Stage 2: Bypassing integrity.**

**Figure 5.** An illustration of the two-stage computation integrity attack on Soter. **Stage 1: Subspace Recovery.** The attacker collects two independent sets of vectors from the TEE’s output, Set A and Set B. By computing the intersection of the vector spaces they span, the attacker recovers the secret cornerstone fingerprint subspace ( $V_C$ ). **Stage 2: Integrity Bypass.** The attacker intercepts a new query (4), uses the recovered subspace as a filter to identify the challenge fingerprints.

now distinguish the fingerprints from genuine activations. Using this knowledge, the attacker only tampers the genuine activations while correctly computing the integrity checks.

**5.1.1 Stage 1: Revealing the subspace for  $m_i$ .** The attacker begins by passively monitoring the TEE-GPU interface to collect two independent sets of outputs, Set A (1) and Set B (2). Each set itself is generated from  $K + \delta$  independent inference calls. For Soter,  $K = 10$ . Because each challenge is generated from a fresh, random linear combination of all cornerstone fingerprints,  $K + \delta$  calls for each set ensure that the cornerstone fingerprint subspace is a subspace of the vector space spanned by each set. The inference calls are kept independent of each other to avoid any linear dependence within the genuine activations. Therefore, the only structure systematically shared between the two sets is

the underlying static cornerstone subspace,  $V_C$ . The adversary recovers a basis for  $V_C$  by computing the intersection of the vector spaces spanned by set  $A$  and set  $B$  (3). Note that the individual fingerprint vectors within set  $A$  will be different from those within set  $B$ . We can still calculate the intersection subspace because even though these fingerprint vectors are distinct, those within set  $A$  and those within set  $B$  each span the cornerstone fingerprint subspace  $V_C$ . Calculating the subspace intersection reduces to solving a system of linear equations (Appendix B).

### 5.1.2 Stage 2: Identifying the fingerprint to bypass the integrity check.

Once the attacker has uncovered the fingerprint subspace,  $V_C$ , they use it to bypass the integrity checks as follows:

- If a vector lies inside the subspace  $V_C$ , it is identified as an integrity challenge. To remain undetected, the attacker allows it to be processed correctly, passing the integrity check.
- If a vector lies outside the subspace  $V_C$ , it is identified as a genuine user query. The attacker is now free to return a tampered result to the application 6.

This attack fully compromises Soter’s integrity mechanism, demonstrating that the efficiency-driven static basis design pattern is insecure even in sophisticated protocols.

## 6 Evaluation

In this section, we empirically validate the feasibility and effectiveness of our proposed attacks. Our evaluation is structured to answer six key questions:

**RQ1:** Why is the vulnerable precomputation pattern a necessary choice for designers? (§6.2)

**RQ2:** Can an attacker discover the secret noise dimension,  $K$ , to get a foothold? (§6.3)

**RQ3:** How effective are the attacks once the prerequisite knowledge is obtained? (§6.4)

**RQ4:** Are the attacks robust against simple countermeasures like random subset sampling or increasing  $K$ ? (§6.5)

**RQ5:** Are the attacks practical and scalable against large, state-of-the-art models? (§6.6)

**RQ6:** What is the final impact of a successful attack on the model’s IP? (§6.7)

### 6.1 Experimental Setup

**Setup.** Our experiments are conducted on a server with a dual-socket Intel Xeon Silver 4309Y CPU (2.80 GHz, SGXv2 enabled with a 4 GB EPC, of which 512 MB is allocated as heap space for our enclave) and a colocated NVIDIA A100-80GB GPU. The software stack consists of Rocky Linux 9.5, Intel SGX SDK v2.25, and PyTorch 2.5.1.

**Implementation.** Our implementation consists of two components. First, for the real-world performance benchmarks (RQ1, RQ6), we built a lightweight, single-threaded C++ library to execute the TEE-based cryptographic protocols on our physical SGX hardware. This library implements standard optimizations like fast modular reduction and memory tiling. Second, for a controlled analysis of the protocol-level vulnerabilities (RQ2–RQ6), we implemented faithful simulations of the core protocols from TLG and Soter. All finite field  $\mathbb{F}_P$  computations are done with the prime  $P = 2^{31}-1$  unless stated otherwise. For the integrity attack simulation, we assume activations are drawn from a normal distribution.

### 6.2 The Performance Imperative for Precomputation

Our central claim is that the static basis vulnerability arises from a severe security-performance trade-off. To validate this premise, we first benchmark the performance of a TEE-shielded LLaMA-3 8B model. We implement the TEE-based model confidentiality protocol presented in TLG, as detailed in Section 2.1. To compute the noise,  $m$ , and its noise effect,  $mW_3$  (6 and 8 in Figure 3), we compare two cryptographic strategies analyzed in Section 3: a secure on-the-fly method that generates fresh randomness for each operation, and the precomputation method that uses a static basis.

As shown in Figure 6, the secure on-the-fly noise generation method is 37x - 55x slower than the precomputation strategy. For a typical interactive scenario (batch size 1, 128-token prompt), the on-the-fly method has a time-to-first-token (TTFT) of 187 seconds, compared to 3.61 seconds for the precomputation strategy. This is a 52x slowdown, making it unsuitable for real-world applications. The impact on throughput is also severe. At a batch size of 8, the on-the-fly method achieves only 0.5 tokens/sec (TPS), while the precomputation strategy delivers 18.6 TPS. This prohibitive performance gap makes the secure on-the-fly method impractical for any system requiring low-latency inference.

**Answer to RQ1:** The secure on-the-fly method imposes prohibitive performance costs on TTFT and TPS. This effectively pushes designers to use the faster but vulnerable precomputation approach.

### 6.3 Discoverability of Secret Noise Dimension $K$

A key artifact of the static basis vulnerability is that the secret noise dimension,  $K$ , is empirically observable. While our threat model grants the attacker knowledge of this parameter, we first demonstrate it can be discovered empirically. This initial step showcases how the core algebraic principles of our attack serve as a versatile method to snoop for information leakage inherent to the precomputation-based pattern. We show this for both of our target systems.

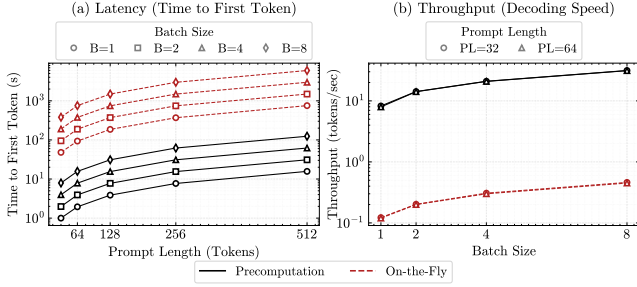


**Figure 6.** Performance comparison demonstrating the security-performance tension. The secure on-the-fly mitigation exhibits (a) orders-of-magnitude higher latency and (b) lower throughput than the vulnerable precomputation system, rendering it impractical for real-world use.

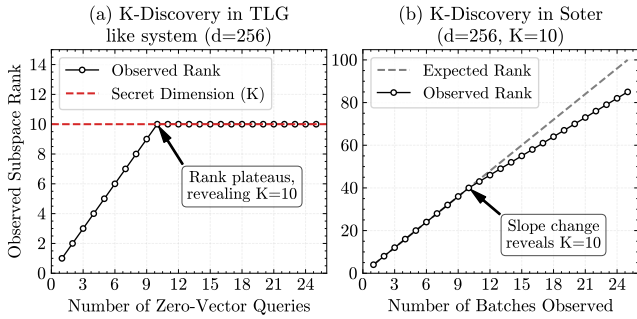


**Figure 7.** Empirical discovery of the secret noise dimension  $K$ . (a) In the direct system, the rank of observed outputs stabilizes at  $K=10$ . (b) In the hidden system (Soter), a distinct change in the slope of rank growth reveals  $K=10$ .

For a TLG-like system, an attacker can perform the first stage of the attack described in Section 4 by sending zero-vector queries (1 in Figure 4) and observing the rank of the resulting output vectors. As shown in Figure 7 (a), the rank grows linearly with each new observation until it stabilizes precisely at  $K$ , which reveals the system parameter.

For a more complex system like Soter, an attacker can passively execute the first part of the subspace recovery stage of the attack detailed in Section 5. As the attacker observes batches of mixed data (1 in Figure 5), the rank of the collected vectors initially grows linearly. However, as shown in Figure 7(b), the rank growth soon deviates from the expected trajectory, revealing a distinct change in slope. This occurs because the low-dimensional fingerprints, all drawn from the same precomputed basis, contribute progressively less new information. This deviation allows an attacker to infer the dimension of the fingerprint subspace,  $K$ .

**Answer to RQ2:** Yes,  $K$  is leaked in both systems. An active attacker can discover  $K$  in a TLG-like system by observing the output rank plateauing, similarly for Soter-like systems.

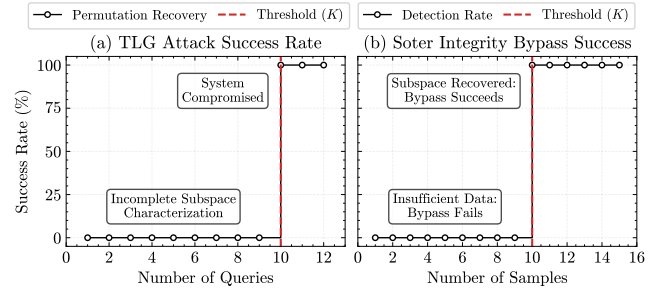


**Figure 8.** This figure plots the success rate of the full attack (Stage 2) as a function of the number of queries used in the initial subspace learning stage (Stage 1). The attack is completely ineffective if the noise subspace is not fully characterized. Once Stage 1 is completed with at least  $K$  queries, the final success rate for a full compromise jumps to 100%.

#### 6.4 Efficacy: A Deterministic and Total System Break

Having established that an attacker can discover  $K$ , we now demonstrate the attack’s efficacy. The success of the final attack is critically dependent on the initial stage of learning the complete noise subspace. To show this, we measure the success rate of the full attack (Stage 1 + Stage 2) while varying the number of queries used to learn the subspace (Stage 1).

The results, shown in Figure 8, reveal a sharp threshold. For our attack on a TLG-like system (a), the final permutation recovery is ineffective when the noise subspace is characterized with fewer than  $K$  queries (1 in Figure 4). However, once the subspace is learned with exactly  $K$  queries, the success rate of the final attack stage jumps to 100%. This demonstrates that fully characterizing the noise subspace is the essential prerequisite for a successful compromise. A similar deterministic threshold is observed for our attack on Soter’s integrity mechanism (b). By observing  $K$  samples for each of its two sets (1 in Figure 5), an attacker can fully recover the cornerstone subspace and reliably distinguish genuine activations from integrity checks.

**Answer to RQ3:** The attacks are 100% effective. They exhibit a sharp, deterministic threshold, transitioning from 0% to 100% success for a full compromise the moment the noise subspace is fully characterized.

#### 6.5 Robustness Against Countermeasures

A robust attack must hold up against plausible defenses. We test our attacks against two intuitive countermeasures: (1) using a more complex random subset sampling to generate noise, and (2) increasing the size of the static basis,  $K$ .

First, we evaluate the random subset sampling strategy, where for each query, the TEE generates noise from a random subset of  $T$  basis vectors ( $T < K$ ). As shown in Figures 9 and 10, this defense is ineffective. The secret dimension  $K$  remains discoverable (Panel (a) in both figures), and the

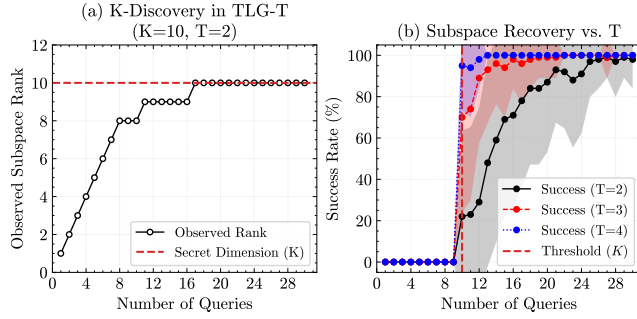


**Figure 9.** Our attack on TLG’s model confidentiality protocol remains effective against a sampling strategy that first chooses  $T$  out of  $K$  noise vectors. (a) An attacker can still discover the secret dimension  $K$  by observing the rank plateau of noise samples. (b) Although smaller  $T$  values require more samples, the attacker can still achieve a 100% success rate in recovering the full noise subspace.

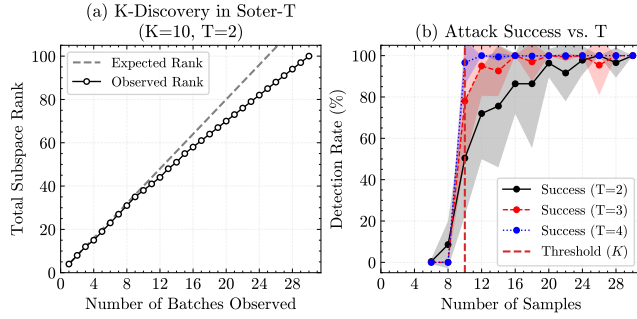


**Figure 10.** Our attack on Soter’s integrity checking mechanism remains effective even against different sampling strategies. (a) The secret dimension  $K$  is still discoverable from rank growth deviation, and (b) while requiring more samples for smaller  $T$ , the attack reliably converges to a 100% success rate, proving the defense is ineffective.

attack’s success rate still reliably converges to 100% (Panel (b) in both figures), albeit with more samples.

Second, we evaluate the strategy of increasing the basis size  $K$ . Figures 11 and 12(b) show this is also futile. The attack success rate remains at 100% regardless of  $K$ . The only effect is that the time-to-compromise scales linearly and predictably with  $K$ .

Both experiments demonstrate that these countermeasures do not fix the fundamental flaw. Increasing  $K$  only makes the attack more expensive, and subset sampling only makes it less efficient, but neither prevents the break.

**Answer to RQ4:** The attacks are robust. Countermeasures like random subset sampling or increasing  $K$  are ineffective.

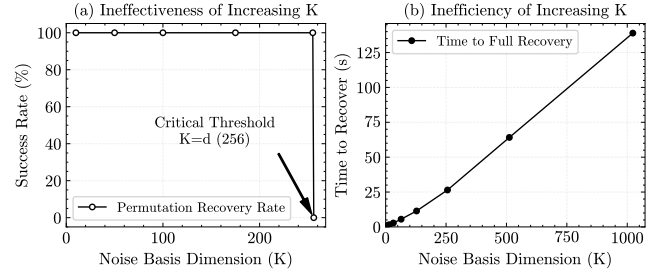


**Figure 11.** Analysis of increasing the noise basis size ( $K$ ) as a defense against the attack on TLG’s model confidentiality protocol. (a) The attack success rate remains at 100%, proving that increasing  $K$  is an ineffective countermeasure. (b) The time-to-attack scales linearly, showing that this defense only predictably delays the compromise.

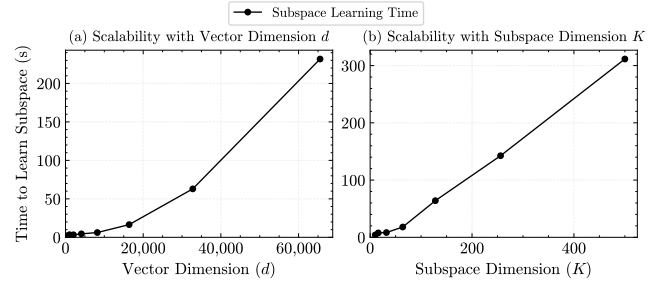


**Figure 12.** Scalability of the attack on Soter’s integrity checking mechanism. The time required to learn the secret subspace scales predictably with both (a) the vector dimension  $d$  and (b) the subspace dimension  $K$ .

## 6.6 Scalability and Practicality: A Real-World Threat

A viable attack must be feasible against large, real-world targets. Here, we analyze the scalability of our attacks to demonstrate their practicality. The primary evidence of practicality is the time-to-compromise. Table 4 details the time required to recover a single layer’s secret permutation for several state-of-the-art LLMs secured using TLG with a precomputation-based approach. The results show that the threat is highly practical: for a model like LLaMA-3 8B, this process takes approximately 6.2 minutes. Even for a massive 405B parameter model, a single layer’s secrets can be recovered in under two hours. These timings were achieved with a single-threaded proof-of-concept implementation. As the attack’s core linear algebra is inherently parallelizable [9, 23], a dedicated attacker could be significantly faster.

Furthermore, our integrity attack on Soter exhibits similarly manageable scaling. As shown in Figure 12(a), the time required to learn the integrity secret subspace also scales predictably and polynomially with the model’s vector dimension,  $d$ . This reinforces that the underlying vulnerability is consistently exploitable at scale across different systems.

**Answer to RQ5:** Yes, the attacks are highly practical. The confidentiality attack can recover a full layer’s secrets in approximately 6.2 minutes for a LLaMA-3 8B model and in under 101 minutes for a 405B model. The integrity attack shows similarly predictable, polynomial scaling.

Model	Dimension ( $d$ )	Required Queries	Time-to-Attack (min)
LLaMA-3 8B	14336	14346	$\approx 6.2$
Gemma 3 27B	21504	21514	$\approx 14.3$
LLaMA-3 70B	28672	28682	$\approx 25.4$
LLAMA-3.1 405B	53248	53258	$\approx 100.7$

**Table 4.** Attack feasibility across models (K=10).

**6.7 Final Impact: Total IP and Integrity Compromise**  
The final impact of our attacks is a versatile and total compromise of the target system’s security. For the confidentiality attack, Table 5 shows the attacker steals a perfect replica of the secret model, achieving identical accuracy and restoring full native performance. For the integrity attack, successfully recovering the fingerprinting subspace allows an attacker to tamper with any offloaded computation without detection. In both cases, the TEE-based protections are rendered completely ineffective due to the vulnerability arising from the use of precomputed noise.

**Answer to RQ6:** The final impact is a total compromise of both security guarantees. The confidentiality attack yields an exact replica of the secret model, and the integrity attack allows undetected tampering with any offloaded computation.

System Configuration	GSM8K Accuracy (%)	Throughput (tok/s)	TEE Required?
Unprotected Baseline (LLaMA-3 8B)	82.34	240	No
Original TEE-Shielded System	82.34	18	Yes
Attacker-Reconstructed Model	82.34	240	No

**Table 5.** Post-attack fidelity and performance. The attacker’s reconstructed model achieves identical accuracy and performance to the original unprotected baseline, proving a total compromise of the model’s intellectual property.

## 7 Related Work

### 7.1 TEE-Shielded Model Protection

Trusted Execution Environments (TEEs) are a hardware-based solution for protecting proprietary machine learning (ML) models on third-party devices. Early solutions in this area focused on executing the entire model within a secure enclave [7, 27, 44, 55]. While this provides strong security, traditional CPU-based TEEs face severe memory and performance constraints that make this impractical for large models [20, 31, 35, 40, 45, 47, 59, 81]. Newer confidential computing architectures on GPUs and CPUs, such as NVIDIA Hopper Confidential Computing and Arm’s CCA, are beginning to address these limitations by enabling the secure execution of entire large models [1, 17, 69, 96].

To leverage powerful but untrusted hardware accelerators like GPUs, Partial TEE-Shielded Execution (PTSE) approaches have been introduced. A crude PTSE strategy involves model partitioning, where the model is split and only the most sensitive layers are executed within the TEE [49–53, 65]. Sophisticated PTSE strategies involve cryptographic obfuscation [5, 10, 28, 30, 73, 78, 87], where weights are decomposed [62], transformed, masked, or permuted inside the TEE before being offloaded for computation [48, 68, 75]. The performance demands of modern LLMs mean these obfuscation schemes either explicitly adopt a precomputed, static secret basis to accelerate cryptographic operations [68, 74, 87], or would require such a design to scale efficiently, making them susceptible to the same vulnerability [46, 48, 75, 84, 93, 94]. Our work is the first to formally identify this performance-driven design pattern as a fundamental flaw and demonstrate its exploitability through a deterministic, cross-query algebraic attack.

### 7.2 Attack Landscape for Secure Inference

**Orthogonal Attack Vectors.** A significant body of work targets secure inference through vectors orthogonal to our protocol-level analysis. Side-channel attacks exploit hardware-level information leakage like cache timing [8, 43], memory access patterns [90], or power consumption [42] to infer secrets, and have been used to leak user inputs [2, 6, 25, 70, 89, 92] and model secrets [21, 32, 60, 85, 88]. Meanwhile, model extraction aims to steal a model’s functionality by training a substitute on its API outputs [12, 13, 18, 36, 54, 56, 63, 64, 79]. Our attack is fundamentally different: we assume a perfect TEE free from side channels and exploit a mathematical flaw in the security protocol itself, rather than attacking its physical implementation or stealing its learned function.

**Protocol-Level Flaws.** Prior work has also identified protocol-level flaws, but these typically exploit statistical properties of the obfuscated weights to infer shielded components by matching them against a known public model [84, 93, 94]. Consequently, the effectiveness of this class of attacks is limited, as they are predicated on the assumption that the victim model is fine-tuned from a public model. Our attack is fundamentally different. It is algebraic and deterministic; we do not infer secrets from noisy correlations but construct a system of linear equations from multiple queries to solve for the exact secret basis. Our contribution is thus more closely aligned with the well-understood category of vulnerabilities stemming from the reuse of secret keying material [11, 66, 71, 80]. We identify the static secret basis pattern as a new manifestation of this flaw within TEE-shielded ML and are the first to demonstrate how it enables an adversary to aggregate information across queries to algebraically break the system’s security.

## 8 Conclusion

This work identifies the use of a precomputed static basis, an appealing optimization that performance-bound TEE-shielded systems are often forced to adopt, as a fundamental vulnerability. We prove its severity through two distinct algebraic attacks that defeat both confidentiality and integrity guarantees: one fully recovers secret permutations in a TLG-like system, while the other completely bypasses the integrity checks in Soter. Our findings reveal a critical tension between this optimization and provable security, highlighting the need for new protocols that achieve high performance without reusing secret material.

## References

- [1] Sina Abdollahi, Mohammad Maher, Sandra Siby, Marios Kogias, and Hamed Haddadi. 2025. An Early Experience with Confidential Computing Architecture for On-Device Model Protection. <https://doi.org/10.48550/arXiv.2504.08508>
- [2] Andrew Adiletta and Berk Sunar. 2025. Spill The Beans: Exploiting CPU Cache Side-Channels to Leak Tokens from Large Language Models. <https://doi.org/10.48550/arXiv.2505.00817>
- [3] Anthropic. 2025. Meet Claude Anthropic. <https://www.anthropic.com/claude>
- [4] Apple. 2025. Deploying Transformers on the Apple Neural Engine. <https://machinelearning.apple.com/research/neural-engine-transformers>
- [5] Juyang Bai, Md Hafizul Islam Chowdhury, Jingtao Li, Fan Yao, Chaitali Chakrabarti, and Deliang Fan. 2025. Phantom: Privacy-Preserving Deep Neural Network Model Obfuscation in Heterogeneous TEE and GPU System. 5565–5582. <https://www.usenix.org/conference/usenixsecurity25/presentation/bai-juyang>
- [6] Sarbartha Banerjee, Shijia Wei, Prakash Ramrakhyani, and Mohit Tiwari. 2023. Triton: Software-Defined Threat Model for Secure Multi-Tenant ML Inference Accelerators. In *Proceedings of the 12th International Workshop on Hardware and Architectural Support for Security and Privacy (HASP '23)*. Association for Computing Machinery, New York, NY, USA, 19–28. <https://doi.org/10.1145/3623652.3623672>
- [7] Sebastian P. Bayerl, Tommaso Frassetto, Patrick Jauernig, Korbinian Riedhammer, Ahmad-Reza Sadeghi, Thomas Schneider, Emmanuel Stafp, and Christian Weinert. 2020. Offline Model Guard: Secure and Private ML on Mobile Devices. In *2020 Design, Automation & Test in Europe Conference & Exhibition (DATE)*. 460–465. <https://doi.org/10.23919/DATE48585.2020.9116560>
- [8] D. Bernstein. 2005. Cache-timing attacks on AES. <https://www.semanticscholar.org/paper/Cache-timing-attacks-on-AES-Bernstein/352e74019d86163d73618f03429ae452ab429629>
- [9] Laura Susan Blackford, J. Choi, A. Cleary, A. Petitet, R. C. Whaley, J. Demmel, I. Dhillon, K. Stanley, J. Dongarra, S. Hammarling, G. Henry, and D. Walker. 1996. ScalAPACK: a portable linear algebra library for distributed memory computers - design issues and performance. In *Proceedings of the 1996 ACM/IEEE conference on Supercomputing (Supercomputing '96)*. IEEE Computer Society, USA, 5–es. <https://doi.org/10.1145/369028.369038>
- [10] Ida Bruhns, Sebastian Berndt, Jonas Sander, and Thomas Eisenbarth. 2024. Slalom at the Carnival: Privacy-preserving Inference with Masks from Public Knowledge. *IACR Communications in Cryptology* 1, 3 (Oct. 2024). <https://doi.org/10.62056/akp-49qgxq>
- [11] Hanno Böck, Aaron Zauner, Sean Devlin, Juraj Somorovsky, and Philipp Jovanovic. 2016.Nonce-Disrespecting Adversaries: Practical Forgery Attacks on GCM in TLS. <https://www.usenix.org/conference/woot16/workshop-program/presentation/bock>
- [12] Nicholas Carlini, Matthew Jagielski, and Ilya Mironov. 2020. Cryptanalytic Extraction of Neural Network Models. <https://doi.org/10.48550/arXiv.2003.04884>
- [13] Nicholas Carlini, Daniel Paleka, Krishnamurthy Dj Dvijotham, Thomas Steinke, Jonathan Hayase, A. Feder Cooper, Katherine Lee, Matthew Jagielski, Milad Nasr, Arthur Conmy, Itay Yona, Eric Wallace, David Rolnick, and Florian Tramèr. 2024. Stealing Part of a Production Language Model. <https://doi.org/10.48550/arXiv.2403.06634>
- [14] Zerui Cheng, Edoardo Contente, Ben Finch, Oleg Golev, Jonathan Hayase, Andrew Miller, Niusha Moshrefi, Anshul Nasery, Sandeep Nailwal, Swooong Oh, Himanshu Tyagi, and Pramod Viswanath. 2025. Reclaiming "Open AI" – AI Model Serving Can Be Open Access, Yet Monetizable and Loyal. <https://doi.org/10.48550/arXiv.2411.03887>
- [15] Marcin Chrapk, Anjo Vahldiek-Oberwagner, Marcin Spoczynski, Scott Constable, Mona Vij, and Torsten Hoefer. 2024. Fortify Your Foundations: Practical Privacy and Security for Foundation Model Deployments In The Cloud. <https://doi.org/10.48550/arXiv.2410.05930>
- [16] Can Cui, Yunsheng Ma, Xu Cao, Wenqian Ye, Yang Zhou, Kaizhao Liang, Jintai Chen, Juanwu Lu, Zichong Yang, Kuei-Da Liao, Tianren Gao, Erlong Li, Kun Tang, Zhipeng Cao, Tong Zhou, Ao Liu, Xinrui Yan, Shuqi Mei, Jianguo Cao, Ziran Wang, and Chao Zheng. 2024. A Survey on Multimodal Large Language Models for Autonomous Driving. In *2024 IEEE/CVF Winter Conference on Applications of Computer Vision Workshops (WACVW)*. 958–979. <https://doi.org/10.1109/WACVW60836.2024.00106>
- [17] Ben Dong and Qian Wang. 2025. Evaluating the Performance of the DeepSeek Model in Confidential Computing Environment. <https://doi.org/10.48550/arXiv.2502.11347>
- [18] Matthew Finlayson, Xiang Ren, and Swabha Swayamdipta. 2024. Logistics of API-Protected LLMs Leak Proprietary Information. <https://doi.org/10.48550/arXiv.2403.09539>
- [19] Roya Firooz, Johnathan Tucker, Stephen Tian, Anirudha Majumdar, Jiankai Sun, Weiyu Liu, Yuke Zhu, Shuran Song, Ashish Kapoor, Karol Hausman, Brian Ichter, Danny Driess, Jiajun Wu, Cewu Lu, and Mac Schwager. 2023. Foundation Models in Robotics: Applications, Challenges, and the Future. <https://doi.org/10.48550/arXiv.2312.07843>
- [20] Akshay Gangal, Mengmei Ye, and Sheng Wei. 2020. HybridTEE: Secure Mobile DNN Execution Using Hybrid Trusted Execution Environment. In *2020 Asian Hardware Oriented Security and Trust Symposium (AsianHOST)*. 1–6. <https://doi.org/10.1109/AsianHOST51057.2020.9358260>
- [21] Yansong Gao, Huming Qiu, Zhi Zhang, Binghui Wang, Hua Ma, Al-sharif Abuadbba, Minhui Xue, Anmin Fu, and Surya Nepal. 2024. DeepTheft: Stealing DNN Model Architectures through Power Side Channel. IEEE Computer Society, 3311–3326. <https://doi.org/10.1109/SP54263.2024.000250>
- [22] Ran Gilad-Bachrach, Nathan Dowlin, Kim Laine, Kristin Lauter, Michael Naehrig, and John Wernsing. 2016. CryptoNets: Applying Neural Networks to Encrypted Data with High Throughput and Accuracy. In *Proceedings of The 33rd International Conference on Machine Learning*. PMLR, 201–210. <https://proceedings.mlr.press/v48/gilad-bachrach16.html>
- [23] Gene H. Golub and Charles F. Van Loan. 1996. *Matrix computations (3rd ed.)*. Johns Hopkins University Press, USA.
- [24] Google. 2025. Google Gemini. <https://gemini.google.com>
- [25] Karan Grover, Shruti Tople, Shweta Shinde, Ranjita Bhagwan, and Ramachandran Ramjee. 2019. Privado: Practical and Secure DNN Inference with Enclaves. <https://doi.org/10.48550/arXiv.1810.00602>
- [26] Monika Gupta. 2023. Google Tensor G3: The new chip that gives your Pixel an AI upgrade. <https://blog.google/products/pixel/google-tensor-g3-pixel-8/>
- [27] Lucjan Hanzlik, Yang Zhang, Kathrin Grosse, Ahmed Salem, Max Augustin, Michael Backes, and Mario Fritz. 2019. MLCapsule: Guarded Offline Deployment of Machine Learning as a Service. <https://doi.org/10.48550/arXiv.1808.00590>

[28] Hanieh Hashemi, Yongqin Wang, and Murali Annavaram. 2022. DarKnight: An Accelerated Framework for Privacy and Integrity Preserving Deep Learning Using Trusted Hardware. <https://doi.org/10.48550/arXiv.2207.00083>

[29] Sanghyun Hong, Pietro Frigo, Yiğitcan Kaya, Cristiano Giuffrida, and Tudor Dumitras. 2019. Terminal Brain Damage: Exposing the Graceless Degradation in Deep Neural Networks Under Hardware Fault Attacks. 497–514. <https://www.usenix.org/conference/usenixsecurity19/presentation/hong>

[30] Jiahui Hou, Huiqi Liu, Yunxin Liu, Yu Wang, Peng-Jun Wan, and Xiang-Yang Li. 2022. Model Protection: Real-Time Privacy-Preserving Inference Service for Model Privacy at the Edge. *IEEE Transactions on Dependable and Secure Computing* 19, 6 (Nov. 2022), 4270–4284. <https://doi.org/10.1109/TDSC.2021.3126315>

[31] Bin Hu, Yan Wang, Jerry Cheng, Tianming Zhao, Yucheng Xie, Xiaonan Guo, and Yingying Chen. 2023. Secure and Efficient Mobile DNN Using Trusted Execution Environments. In *Proceedings of the 2023 ACM Asia Conference on Computer and Communications Security (ASIA CCS '23)*. Association for Computing Machinery, New York, NY, USA, 274–285. <https://doi.org/10.1145/3579856.3582820>

[32] Weizhe Hua, Zhiru Zhang, and G. Edward Suh. 2018. Reverse engineering convolutional neural networks through side-channel information leaks. In *Proceedings of the 55th Annual Design Automation Conference (DAC '18)*. Association for Computing Machinery, New York, NY, USA, 1–6. <https://doi.org/10.1145/3195970.3196105>

[33] Hanbo Huang, Yihan Li, Bowen Jiang, Lin Liu, Bo Jiang, Ruoyu Sun, Zhiotao Liu, and Shiyu Liang. 2025. Position: On-Premises LLM Deployment Demands a Middle Path: Preserving Privacy Without Sacrificing Model Confidentiality. <https://doi.org/10.48550/arXiv.2410.11182>

[34] Tyler Hunt, Zhipeng Jia, Vance Miller, Ariel Szekely, Yige Hu, Christopher J. Rossbach, and Emmett Witchel. 2020. Telekine: Secure Computing with Cloud GPUs. 817–833. <https://www.usenix.org/conference/nsdi20/presentation/hunt>

[35] Md Shihabul Islam, Mahmoud Zamani, Chung Hwan Kim, Latifur Khan, and Kevin W. Hamlen. 2023. Confidential Execution of Deep Learning Inference at the Untrusted Edge with ARM TrustZone. In *Proceedings of the Thirteenth ACM Conference on Data and Application Security and Privacy (CODASPY '23)*. Association for Computing Machinery, New York, NY, USA, 153–164. <https://doi.org/10.1145/3577923.3583648>

[36] Matthew Jagielski, Nicholas Carlini, David Berthelot, Alex Kurakin, and Nicolas Papernot. 2020. High Accuracy and High Fidelity Extraction of Neural Networks. 1345–1362. <https://www.usenix.org/conference/usenixsecurity20/presentation/jagielski>

[37] Chiraag Juvekar, Vinod Vaikuntanathan, and Anantha Chandrakasan. 2018. {GAZELLE}: A Low Latency Framework for Secure Neural Network Inference. 1651–1669. <https://www.usenix.org/conference/usenixsecurity18/presentation/juvekar>

[38] David Kaplan, Jeremy Powell, and Tom Woller. 2021. *memory-encryption-white-paper*. Technical Report. <https://www.amd.com/content/dam/amd/en/documents/epyc-business-docs/white-papers/memory-encryption-white-paper.pdf>

[39] Leela Karumbunathan. 2022. *nvidia jetson agx orin technical brief*. Technical Report. <https://www.nvidia.com/content/dam/en-zz/Solutions/gtcf21/jetson-orin/nvidia-jetson-agx-orin-technical-brief.pdf>

[40] Kyungtae Kim, Chung Hwan Kim, Junghwan "John" Rhee, Xiao Yu, Haifeng Chen, Dave (Jing) Tian, and Byoungyoung Lee. 2020. Vessels: efficient and scalable deep learning prediction on trusted processors. In *Proceedings of the 11th ACM Symposium on Cloud Computing (SoCC '20)*. Association for Computing Machinery, New York, NY, USA, 462–476. <https://doi.org/10.1145/3419111.3421282>

[41] Yoongu Kim, Ross Daly, Jeremie Kim, Chris Fallin, Ji Hye Lee, Donghyuk Lee, Chris Wilkerson, Konrad Lai, and Onur Mutlu. 2014. Flipping bits in memory without accessing them: an experimental study of DRAM disturbance errors. *SIGARCH Comput. Archit. News* 42, 3 (June 2014), 361–372. <https://doi.org/10.1145/2678373.2665726>

[42] Paul Kocher, Joshua Jaffe, and Benjamin Jun. 1999. Differential Power Analysis. In *Advances in Cryptology — CRYPTO'99*. Michael Wiener (Ed.). Springer, Berlin, Heidelberg, 388–397. [https://doi.org/10.1007/3-540-48405-1\\_25](https://doi.org/10.1007/3-540-48405-1_25)

[43] Paul C. Kocher. 1996. Timing Attacks on Implementations of Diffie-Hellman, RSA, DSS, and Other Systems. In *Advances in Cryptology — CRYPTO '96*. Neal Koblitz (Ed.). Springer, Berlin, Heidelberg, 104–113. [https://doi.org/10.1007/3-540-68697-5\\_9](https://doi.org/10.1007/3-540-68697-5_9)

[44] Roland Kunkel, Do Le Quoc, Franz Gregor, Sergei Arnaudov, Pramod Bhatotia, and Christof Fetzer. 2019. TensorSCONE: A Secure TensorFlow Framework using Intel SGX. <https://doi.org/10.48550/arXiv.1902.04413>

[45] Taegyeong Lee, Zhiqi Lin, Saumay Pushp, Caihua Li, Yunxin Liu, Youngki Lee, Fengyuan Xu, Chenren Xu, Lintao Zhang, and Junehwa Song. 2019. Occlumency: Privacy-preserving Remote Deep-learning Inference Using SGX. In *The 25th Annual International Conference on Mobile Computing and Networking (MobiCom '19)*. Association for Computing Machinery, New York, NY, USA, 1–17. <https://doi.org/10.1145/3300061.3345447>

[46] Ding Li, Ziqi Zhang, Mengyu Yao, Yifeng Cai, Yao Guo, and Xiangqun Chen. 2024. TEESlice: Protecting Sensitive Neural Network Models in Trusted Execution Environments When Attackers have Pre-Trained Models. <https://doi.org/10.48550/arXiv.2411.09945>

[47] Fabin Li, Xiang Li, and Mingyu Gao. 2023. Secure MLaaS with Temper: Trusted and Efficient Model Partitioning and Enclave Reuse. In *Proceedings of the 39th Annual Computer Security Applications Conference (ACSAC '23)*. Association for Computing Machinery, New York, NY, USA, 621–635. <https://doi.org/10.1145/3627106.3627145>

[48] Qinfeng Li, Zhiqiang Shen, Zhenghan Qin, Yangfan Xie, Xuhong Zhang, Tianyu Du, and Jianwei Yin. 2024. TransLinkGuard: Safeguarding Transformer Models Against Model Stealing in Edge Deployment. In *Proceedings of the 32nd ACM International Conference on Multimedia*. 3479–3488. <https://doi.org/10.1145/3664647.3680786>

[49] Ziyu Liu, Yukui Luo, Shijin Duan, Tong Zhou, and Xiaolin Xu. 2023. MirrorNet: A TEE-Friendly Framework for Secure On-device DNN Inference. <https://doi.org/10.48550/arXiv.2311.09489>

[50] Ziyu Liu, Tong Zhou, Yukui Luo, and Xiaolin Xu. 2024. TBNet: A Neural Architectural Defense Framework Facilitating DNN Model Protection in Trusted Execution Environments. <https://doi.org/10.48550/arXiv.2405.03974>

[51] Fan Mo, Ali Shahin Shamsabadi, Kleomenis Katevas, Soteris Demetriadou, Ilias Leontiadis, Andrea Cavallaro, and Hamed Haddadi. 2020. DarknetZ: Towards Model Privacy at the Edge using Trusted Execution Environments. In *Proceedings of the 18th International Conference on Mobile Systems, Applications, and Services*. 161–174. <https://doi.org/10.1145/3386901.3388946>

[52] Fan Mo, Zahra Tarkhani, and Hamed Haddadi. 2024. Machine Learning with Confidential Computing: A Systematization of Knowledge. *ACM Comput. Surv.* 56, 11 (June 2024), 281:1–281:40. <https://doi.org/10.1145/3670007>

[53] Krishna Giri Narra, Zhifeng Lin, Yongqin Wang, Keshav Balasubramanian, and Murali Annavaram. 2019. Privacy-Preserving Inference in Machine Learning Services Using Trusted Execution Environments. <https://doi.org/10.48550/arXiv.1912.03485>

[54] Tushar Nayan, Qiming Guo, and Mohammed Al Duniawi. 2024. SoK: All You Need to Know About On-Device ML Model Extraction - The Gap Between Research and Practice. (2024).

[55] Olga Ohrimenko, Felix Schuster, Cédric Fournet, Aastha Mehta, Sebastian Nowozin, Kapil Vaswani, and Manuel Costa. 2016. Oblivious {Multi-Party} Machine Learning on Trusted Processors. 619–636. <https://www.usenix.org/conference/usenixsecurity16/technical>

sessions/presentation/ohrimenko

[56] Daryna Oliynyk, Rudolf Mayer, Kathrin Grosse, and Andreas Rauber. 2025. I Stolenly Swear That I Am Up to (No) Good: Design and Evaluation of Model Stealing Attacks. <https://doi.org/10.48550/arXiv.2508.21654>

[57] OpenAI. 2025. ChatGPT. <https://chatgpt.com/?locale=en-US>

[58] OpenAI. 2025. ChatGPT for Enterprise. <https://chatgpt.com/business-enterprise/>

[59] Do Le Quoc, Franz Gregor, Sergei Arnautov, Roland Kunkel, Pramod Bhatotia, and Christof Fetzer. 2020. secureTF: A Secure TensorFlow Framework. In *Proceedings of the 21st International Middleware Conference (Middleware '20)*. Association for Computing Machinery, New York, NY, USA, 44–59. <https://doi.org/10.1145/3423211.3425687>

[60] Adnan Siraj Rakin, Md Hafizul Islam Chowdhury, Fan Yao, and Deliang Fan. 2022. DeepSteal: Advanced Model Extractions Leveraging Efficient Weight Stealing in Memories. In *2022 IEEE Symposium on Security and Privacy (SP)*. 1157–1174. <https://doi.org/10.1109/SP46214.2022.9833743>

[61] Adnan Siraj Rakin, Zhezhi He, Jingtao Li, Fan Yao, Chaitali Chakrabarti, and Deliang Fan. 2021. T-BFA: Targeted Bit-Flip Adversarial Weight Attack. <https://doi.org/10.48550/arXiv.2007.12336>

[62] Yehonathan Refael, Adam Hakim, Lev Greenberg, Tal Aviv, Satya Lokam, Ben Fishman, and Shachar Seidman. 2024. SLIP: Securing LLMs IP Using Weights Decomposition. <https://doi.org/10.48550/arXiv.2407.10886>

[63] David Rolnick and Konrad P. Kording. 2019. Reverse-Engineering Deep ReLU Networks. <https://arxiv.org/abs/1910.00744v2>

[64] Sunandini Sanyal, Sravanti Addepalli, and R. Venkatesh Babu. 2022. Towards Data-Free Model Stealing in a Hard Label Setting. <https://doi.org/10.48550/arXiv.2204.11022>

[65] Alexander Schlögl and Rainer Böhme. 2020. eNNclave: Offline Inference with Model Confidentiality. In *Proceedings of the 13th ACM Workshop on Artificial Intelligence and Security (AISeC '20)*. Association for Computing Machinery, New York, NY, USA, 93–104. <https://doi.org/10.1145/3411508.3421376>

[66] Bruce Schneier and Mudge. 1998. Cryptanalysis of Microsoft’s point-to-point tunneling protocol (PPTP). In *Proceedings of the 5th ACM conference on Computer and communications security (CCS '98)*. Association for Computing Machinery, New York, NY, USA, 132–141. <https://doi.org/10.1145/288090.288119>

[67] SentinelOne. 2025. ChatGPT Security Risks: All You Need to Know. <https://www.sentinelone.com/cybersecurity-101/data-and-ai/chatgpt-security-risks/>

[68] Tianxiang Shen, Ji Qi, Jianyu Jiang, Xian Wang, Siyuan Wen, Xusheng Chen, Shixiong Zhao, and Xiapu Luo. 2022. Soter: Guarding Black-box Inference for General Neural Networks at the Edge. (2022).

[69] Sandra Siby, Sina Abdollahi, Mohammad Maher, Marios Kogias, and Hamed Haddadi. 2024. GuarTEE: Towards Attestable and Private ML with CCA. <https://doi.org/10.48550/arXiv.2404.00190>

[70] Tyler Sorensen and Heidy Khlaaf. 2024. LeftoverLocals: Listening to LLM Responses Through Leaked GPU Local Memory. <https://doi.org/10.48550/arXiv.2401.16603>

[71] Douglas Robert Stinson and Maura Paterson. 2018. *Cryptography: Theory and Practice* (4 ed.). Chapman and Hall/CRC, New York.

[72] Ion Stoica, Dawn Song, Raluca Ada Popa, David A. Patterson, Michael W. Mahoney, Randy H. Katz, Anthony D. Joseph, Michael Jordan, Joseph M. Hellerstein, Joseph Gonzalez, Ken Goldberg, Ali Ghodsi, David E. Culler, and Pieter Abbeel. 2017. *A Berkeley View of Systems Challenges for AI*. Technical Report UCB/EECS-2017-159. <http://www2.eecs.berkeley.edu/Pubs/TechRpts/2017/EECS-2017-159.html>

[73] Tong Sun, Bowen Jiang, Hailong Lin, Borui Li, Yixiao Teng, Yi Gao, and Wei Dong. 2025. TensorShield: Safeguarding On-Device Inference by Shielding Critical DNN Tensors with TEE. <https://doi.org/10.48550/arXiv.2505.22735>

[74] Yu Sun, Gaojian Xiong, Jianhua Liu, Zheng Liu, and Jian Cui. 2025. TSQP: Safeguarding Real-Time Inference for Quantization Neural Networks on Edge Devices. In *2025 IEEE Symposium on Security and Privacy (SP)*. IEEE Computer Society, Los Alamitos, CA, USA, 2114–2132. <https://doi.org/10.1109/SP61157.2025.00001>

[75] Zhichuang Sun, Ruimin Sun, Changming Liu, Amrita Roy Chowdhury, Long Lu, and Somesh Jha. 2023. ShadowNet: A Secure and Efficient On-device Model Inference System for Convolutional Neural Networks. <https://doi.org/10.48550/arXiv.2011.05905>

[76] Zhichuang Sun, Ruimin Sun, Long Lu, and Alan Mislove. 2021. Mind Your Weight(s): A Large-scale Study on Insufficient Machine Learning Model Protection in Mobile Apps. <https://doi.org/10.48550/arXiv.2002.07687>

[77] Tesla. 2025. Autopilot | Tesla Support. <https://www.tesla.com/support/autopilot>

[78] Florian Tramèr and Dan Boneh. 2019. Slalom: Fast, Verifiable and Private Execution of Neural Networks in Trusted Hardware. <https://doi.org/10.48550/arXiv.1806.03287>

[79] Florian Tramèr, Fan Zhang, Ari Juels, Michael K. Reiter, and Thomas Ristenpart. 2016. Stealing Machine Learning Models via Prediction APIs. <https://doi.org/10.48550/arXiv.1609.02943>

[80] Mathy Vanhoef and Frank Piessens. 2017. Key Reinstallation Attacks: ForcingNonce Reuse in WPA2. In *Proceedings of the 2017 ACM SIGSAC Conference on Computer and Communications Security (CCS '17)*. Association for Computing Machinery, New York, NY, USA, 1313–1328. <https://doi.org/10.1145/3133956.3134027>

[81] Peter M. VanNostrand, Ioannis Kyriazis, Michelle Cheng, Tian Guo, and Robert J. Walls. 2019. Confidential Deep Learning: Executing Proprietary Models on Untrusted Devices. <https://doi.org/10.48550/arXiv.1908.10730>

[82] Kapil Vaswani, Stavros Volos, Cédric Fournet, Antonio Nino Diaz, Ken Gordon, Balaji Vembu, Sam Webster, David Chisnall, Saurabh Kulkarni, Graham Cunningham, Richard Osborne, and Daniel Wilkinson. 2023. Confidential Computing within an AI Accelerator. 501–518. <https://www.usenix.org/conference/atc23/presentation/vaswani>

[83] Stavros Volos, Kapil Vaswani, and Rodrigo Bruno. 2018. Graviton: Trusted Execution Environments on GPUs. 681–696. <https://www.usenix.org/conference/osdi18/presentation/volos>

[84] Pengli Wang. 2025. Game of Arrows: On the (In-)Security of Weight Obfuscation for On-Device TEE-Shielded LLM Partition Algorithms. (2025).

[85] Junyi Wei, Yicheng Zhang, Zhe Zhou, Zhou Li, and Mohammad Abdullah Al Faruque. 2020. Leaky DNN: Stealing Deep-Learning Model Secret with GPU Context-Switching Side-Channel. In *2020 50th Annual IEEE/IFIP International Conference on Dependable Systems and Networks (DSN)*. 125–137. <https://doi.org/10.1109/DSN48063.2020.00031>

[86] Henry Wilhelm. 2023. Amazon unveils a new lineup of Echo devices—here’s your first look. <https://www.aboutamazon.com/news/devices/new-amazon-echo-devices-echo-buds-echo-pop>

[87] Rongwu Xu and Zhixuan Fang. 2024. Tempo: Confidentiality Preservation in Cloud-Based Neural Network Training. <https://doi.org/10.48550/arXiv.2401.11531>

[88] Mengjia Yan, Christopher W. Fletcher, and Josep Torrellas. 2020. Cache Telepathy: Leveraging Shared Resource Attacks to Learn DNN Architectures. 2003–2020. <https://www.usenix.org/conference/usenixsecurity20/presentation/yan>

[89] Huan Yang, Deyu Zhang, Yudong Zhao, Yuanchun Li, and Yunxin Liu. 2024. A First Look At Efficient And Secure On-Device LLM Inference Against KV Leakage. <https://doi.org/10.48550/arXiv.2409.04040>

[90] Yuval Yarom and Katrina Falkner. 2014. FLUSH+RELOAD: A High Resolution, Low Noise, L3 Cache Side-Channel Attack. 719–732. <https://www.usenix.org/conference/usenixsecurity14/technical-sessions/presentation/yarom>

- [91] Mu Yuan, Lan Zhang, and Xiang-Yang Li. 2024. Secure Transformer Inference Protocol. <https://doi.org/10.48550/arXiv.2312.00025>
- [92] Yuanyuan Yuan, Zhibo Liu, Sen Deng, Yanzuo Chen, Shuai Wang, Yin-qian Zhang, and Zhendong Su. 2024. CipherSteal: Stealing Input Data from TEE-Shielded Neural Networks with Ciphertext Side Channels. IEEE Computer Society, 4136–4154. <https://doi.org/10.1109/SP61157.2025.00079>
- [93] Ziqi Zhang, Chen Gong, Yifeng Cai, Yuanyuan Yuan, Bingyan Liu, Ding Li, Yao Guo, and Xiangqun Chen. 2023. No Privacy Left Outside: On the (In-)Security of TEE-Shielded DNN Partition for On-Device ML. <https://doi.org/10.48550/arXiv.2310.07152>
- [94] Zheng Zhang, Na Wang, Ziqi Zhang, Yao Zhang, Tianyi Zhang, Jianwei Liu, and Ye Wu. 2024. GroupCover: A Secure, Efficient and Scalable Inference Framework for On-device Model Protection based on TEEs. In *Proceedings of the 41st International Conference on Machine Learning*. PMLR, 59992–60003. <https://proceedings.mlr.press/v235/zhang24bn.html>
- [95] Pu Zhao, Siyue Wang, Cheng Gongye, Yanzhi Wang, Yunsi Fei, and Xue Lin. 2019. Fault Sneaking Attack: a Stealthy Framework for Misleading Deep Neural Networks. In *Proceedings of the 56th Annual Design Automation Conference 2019 (DAC '19)*. Association for Computing Machinery, New York, NY, USA, 1–6. <https://doi.org/10.1145/3316781.3317825>
- [96] Jianwei Zhu, Hang Yin, Peng Deng, Aline Almeida, and Shunfan Zhou. 2024. Confidential Computing on NVIDIA Hopper GPUs: A Performance Benchmark Study. <https://doi.org/10.48550/arXiv.2409.03992>

## A Appendix: Derivation of the Rank Deficiency Probability

We want to find the probability that a randomly generated  $K \times K$  matrix  $M$ , whose entries are chosen uniformly from a finite field  $\mathbb{F}_P$  with  $P$  elements (i.e., each entry of matrix  $M$  can be any integer from 0 to  $P - 1$  with equal probability), is rank deficient (i.e., singular or has columns that are linearly dependent).

It is easier to first calculate the probability of the complementary event: that the matrix  $M$  has **full rank** (i.e., is invertible). We can then find the desired probability using the relation:

$$P(\text{rank deficient}) = 1 - P(\text{full rank})$$

Using the chain rule of probability, we can express this probability as:

$$\begin{aligned} P(\text{full rank}) &= P(K \text{ cols are independent}) \\ &= P(\text{col } K \text{ is indep.} \mid \text{first } K - 1 \text{ are indep.}) \\ &\quad \times P(\text{first } K - 1 \text{ cols are indep.}) \\ &= P(\text{col } K \text{ is indep.} \mid \text{first } K - 1 \text{ are indep.}) \\ &\quad \times P(\text{col } K - 1 \text{ is indep.} \mid \text{first } K - 2 \text{ are indep.}) \\ &\quad \times P(\text{first } K - 2 \text{ cols are indep.}) \end{aligned}$$

Expanding this further, we get,

$$P(\text{full rank}) = \prod_{i=1}^K P(\text{col } i \text{ is indep.} \mid \text{first } i - 1 \text{ are indep.})$$

Next, we will find  $P(\text{col } i \text{ is indep.} \mid \text{first } i - 1 \text{ are indep.})$  and plug it back into the previous equation. Next,

$$\begin{aligned} P(\text{col } i \text{ is indep.} \mid \text{first } i - 1 \text{ are indep.}) &= \frac{P^K - P^{i-1}}{P^K} \\ &= 1 - \frac{P^{i-1}}{P^K} \end{aligned}$$

This is because  $P^K$  is the total number of possibilities for the new column since each of the  $K$  entries can take any value from 0 to  $P - 1$ . Out of these, we subtract the number of entries that will be a linear combination of the previously selected  $i - 1$  columns. Each such linear combination can be written as  $\alpha_1 c_1 + \alpha_2 c_2 + \dots + \alpha_{i-1} c_{i-1}$ , where  $c_1, c_2, \dots, c_{i-1}$  are the  $i - 1$  columns and  $\alpha_1, \alpha_2, \dots, \alpha_{i-1}$  are the coefficients the columns are multiplied by to generate the linear combination. Each distinct value of the coefficients  $\alpha_1, \alpha_2, \dots, \alpha_{i-1}$  gives a distinct vector (because the previous columns are linearly independent), and there are  $P^{i-1}$  such possibilities.

Substituting this back into the equation for  $P(\text{full rank})$ , we get,

$$P(\text{full rank}) = \prod_{i=1}^K \left(1 - \frac{P^{i-1}}{P^K}\right)$$

$$= \left(1 - \frac{P^0}{P^K}\right) \left(1 - \frac{P^1}{P^K}\right) \cdots \left(1 - \frac{P^{K-1}}{P^K}\right)$$

Re-indexing with  $j = K - (i - 1)$ , this product simplifies to:

$$P(\text{full rank}) = \prod_{j=1}^K \left(1 - \frac{1}{P^j}\right)$$

Finally, the probability of being rank deficient is the complement:

$$P(\text{rank deficient}) = 1 - P(\text{full rank}) = 1 - \prod_{i=1}^K \left(1 - \frac{1}{P^i}\right)$$

## B Intersection of Vector Spaces

Additionally, calculating the intersection of two subspaces can be done by solving a system of linear equations. Therefore, it is computationally feasible as it can be done in polynomial time. We briefly discuss how one can compute the intersection of two sets of vectors  $U = \{u_1, u_2, \dots, u_m\}$  and  $W = \{w_1, w_2, \dots, w_n\}$  consisting of  $n$  and  $m$  vectors, respectively. Suppose a vector,  $v$ , is in the intersection of the subspaces spanned by  $U$  and  $W$ . Then it can be written as a linear combination of the vectors in both  $U$  and  $W$ . Thus, we can write,

$$v = \gamma_1 u_1 + \gamma_2 u_2 + \dots + \gamma_m u_m = \delta_1 w_1 + \delta_2 w_2 + \dots + \delta_n w_n \quad (1)$$

where  $\gamma_1, \gamma_2, \dots, \gamma_m$  and  $\delta_1, \delta_2, \dots, \delta_n$  are the scalar coefficients of the respective linear combinations. To find all such  $v$ , one needs to find all the solutions to Equation 1 and plug them back in to get  $v$ . Solving Equation 1 is equivalent to solving the system of linear equation below,

$$\gamma_1 u_1 + \gamma_2 u_2 + \dots + \gamma_m u_m = \delta_1 w_1 + \delta_2 w_2 + \dots + \delta_n w_n$$

$$\gamma_1 u_1 + \gamma_2 u_2 + \dots + \gamma_m u_m - \delta_1 w_1 - \delta_2 w_2 - \dots - \delta_n w_n = 0$$

This can be condensed into the matrix format as

$$U\vec{\gamma} - W\vec{\delta} = 0$$

$$\begin{bmatrix} U & W \end{bmatrix} \begin{bmatrix} \vec{\gamma} \\ \vec{\delta} \end{bmatrix} = 0$$

This can be solved by using standard linear algebra techniques like Gaussian Elimination. The solutions can then be plugged back into  $v = U\vec{\gamma}$  to get all possible  $v$ , which will give the intersection subspace.

## C Discussion

The successful attacks detailed in Sections 4 and 5 are more than specific flaws; they are practical demonstrations of a fundamental vulnerability pattern that arises when TEE-based systems prioritize performance via precomputation. The reuse of a static secret across multiple queries creates a structural dependency that allows an adversary to aggregate outputs and break the system. This section discusses the

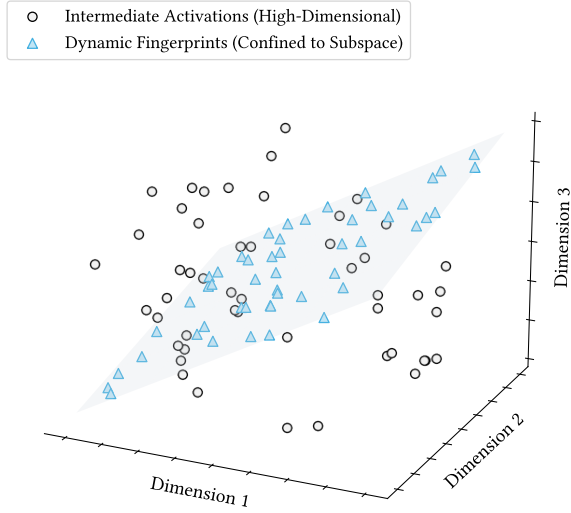


**Figure 13.** A visualization of the root cause of the vulnerability in Soter’s integrity checking mechanism. The generated fingerprints (blue triangles) are confined to a low-dimensional subspace (gray plane) and are thus distinguishable from high-dimensional activations (gray circles).

scope of our findings and outlines potential paths forward for designing more robust systems.

### C.1 Limitations and Scope

It is important to clarify the boundaries of our work. First, our threat model assumes the TEE itself is a secure black box. Our attacks are at the protocol level and do not consider hardware side-channel vulnerabilities that could leak secrets directly from the enclave.

Second, we do not analyze adaptive or behavioral countermeasures. A system could, in theory, monitor for anomalous query patterns (such as repeated zero-vector inputs) and respond by rate-limiting or terminating a session. While such defenses could make our attacks more difficult to execute, they would not fix the underlying cryptographic flaw in the protocol.

### C.2 Paths Forward and Future Directions

Our findings motivate the search for secure, high-performance alternatives to the static basis pattern. One potential mitigation is **remote noise generation**, where a trusted server provides the on-device TEE with batches of single-use, pre-computed noise effects. While this approach solves the static basis vulnerability, it has significant drawbacks: the system is no longer self-contained, and it becomes dependent on network availability and performance.

This analysis, combined with the failures of the systems we studied, leads to a set of core principles for future designs and highlights a key challenge for the community.

#### C.2.1 Design Principles.

**1. Eliminate Reused Static Secrets.** The central lesson of our work is that any secret material reused across queries is a potential liability. Future protocols must prioritize cryptographic designs that ensure forward secrecy by using a dynamic and non-reconstructible basis for each query.

**2. Ensure Obfuscation Resists Cross-Query Analysis.**

The attack on Soter proves that simply mixing a static secret basis with other high-dimensional data is an inadequate defense. A robust defense must ensure that no learnable structure persists across interactions that an adversary can aggregate.

The vulnerability of protocols that rely on a static secret basis motivates the search for a secure alternative. Any robust solution must use a sufficiently dynamic, non-reconstructible noise basis  $N_i$  for each query. The core difficulty lies in how the TEE can obtain the corresponding noise effect  $N_i W'$  efficiently. We discuss two primary mitigation paths for achieving this, each with significant trade-offs.

**C.2.2 Open Research Challenge.** The core difficulty in this domain remains reconciling the tension between performance and security. The ultimate goal is to design a protocol that is simultaneously performant and uses fresh randomness for every query. Achieving this will likely require new cryptographic primitives or hardware-software co-designs that can efficiently compute the effect of fresh noise without the prohibitive cost of on-the-fly matrix multiplication. Solving this challenge remains a critical direction for future research.

## D Algorithms

---

### Algorithm 1. Direct Subspace Characterization Attack

#### Input:

$\text{TEE}(a)$  that returns  $y \in \mathbb{F}_p^d$  for input  $a \in \mathbb{F}_p^d$ .

$K$ : Number of precomputed noise vectors.

$d$ : Dimensionality of embedding vectors.

$P$ : A prime such that integers mod  $P$  form  $\mathbb{F}_P$ .

#### Output:

Recovered permutation  $\hat{\pi} : \{0, \dots, \dim - 1\} \rightarrow \{0, \dots, \dim - 1\}$ .

```

1: /* Generate the subspace  $S_{obs}$  spanned by the  $K$  permuted
   noise vectors */
2:  $Y_{samples} \leftarrow \emptyset$ 
3:  $a_{zero} \leftarrow 0 \in \mathbb{F}_p^{dim}$ 
4: for  $q \leftarrow 1$  to  $K$  do
5:   /* Sample a random vector from subspace  $S_{obs}$ . */
6:   /*  $\text{TEE}(a_{zero}) = \pi(a_{zero} + m) = \pi m$ , where  $m$  is a */
7:   /* random linear combination of the noise vectors. */
8:    $y_q \leftarrow \text{TEE}(a_{zero})$ 
9:   Add  $y_q$  to  $Y_{samples}$ 
10: end for
11:  $\mathcal{B}_{S_{obs}} \leftarrow \text{COMPUTEBASIS}(Y_{samples})$ 

```

```

12: /* Compute a projection to the orthogonal complement of
   the subspace  $S_{obs}$  */
13:  $\text{Proj}_{S_{obs}^\perp} \leftarrow \text{CREATEORTHOGONALCOMPLEMENT}(\mathcal{B}_{S_{obs}})$ 
14: Initialize  $\hat{\pi}[0 \dots \text{dim} - 1] \leftarrow -1$ 
15: for  $j \leftarrow 0$  to  $\text{dim} - 1$  do
16:    $\mathbf{e}_j \leftarrow \text{CREATECANONICALVECTOR}(j, d)$ 
17:    $\mathbf{y}_j \leftarrow \text{TEE}(\mathbf{e}_j)$ 
18:    $\mathbf{s}_j \leftarrow \text{Proj}_{S_{obs}^\perp}(\mathbf{y}_j)$ 
19:   /* Projection cancels noise: */
20:   /*  $\mathbf{s}_j = \text{Proj}_{S_{obs}^\perp}(\mathbf{y}_j) = \text{Proj}_{S_{obs}^\perp}(\pi(\mathbf{e}_j + \mathbf{m}))$  */
21:   /*  $= \text{Proj}_{S_{obs}^\perp}(\pi \mathbf{e}_j) \quad \because \pi \mathbf{m} \in S_{obs}$  */
22:    $\hat{\pi}[j] \leftarrow \text{FINDCOLUMNINDEX}(\text{Proj}_{S_{obs}^\perp}, \mathbf{s}_j)$ 
23: end for

24: return  $\hat{\pi}$ 

```

---

**Algorithm 2.** Integrity Bypass Attack on Soter-like Systems**Input:**

`ObserveInferenceBatch()` that returns a batch of vectors from the TEE.

$k$ : The dimension of the secret cornerstone basis.

$d$ : The dimensionality of the vectors.

```

/* Stage 1: Recover Cornerstone Fingerprint Subspace  $V_C$ 
 */
1: CollectedVectorsA  $\leftarrow \emptyset$ 
2: CollectedVectorsB  $\leftarrow \emptyset$ 
3: /* Passively observe  $k + \delta$  batches for each set to ensure
   they span the subspace */
4: for  $i \leftarrow 1$  to  $k + \delta$  do
5:   batchA  $\leftarrow \text{OBSERVEINFERENCETRACE}$ 
6:   batchB  $\leftarrow \text{OBSERVEINFERENCETRACE}$ 
7:   Add all vectors from batchA to CollectedVectorsA
8:   Add all vectors from batchB to CollectedVectorsB
9: end for
10:  $\mathcal{B}_{U_A} \leftarrow \text{COMPUTEBASIS}(\text{CollectedVectorsA})$ 
11:  $\mathcal{B}_{U_B} \leftarrow \text{COMPUTEBASIS}(\text{CollectedVectorsB})$ 

12: /* The cornerstone subspace is the intersection of the vector
   spaces spanned by the two sets. */
13:  $\mathcal{B}_{V_C} \leftarrow \text{SUBSPACEINTERSECTION}(\mathcal{B}_{U_A}, \mathcal{B}_{U_B})$ 

14: /* Stage 2: Identify Fingerprints to Bypass Integrity Checks
 */

```

```

15: function BYPASSINTEGRITYCHECK(new_batch,  $\mathcal{B}_{V_C}$ )
16:   for each  $\mathbf{v}$  in new_batch do
17:     if ISINSUBSPACE( $\mathbf{v}, \mathcal{B}_{V_C}$ ) then
18:       /* Vector is a fingerprint; process it correctly to
          pass the check. */
19:       RETURNCORRECTRESULT( $\mathbf{v}$ )

```

```

20:     else
21:       /* Vector is genuine data; return a tampered
          result. */
22:       RETURNTAMPEREDRESULT( $\mathbf{v}$ )
23:     end if
24:   end for
25: end function

```

---